MORPHOLOGICAL ADAPTATIONS OF THE SAND-SWIMMER LIZARD *CALYPTOMMATUS LEIOLEPIS* (SQUAMATA: GYMNOPHTHALMIDAE)

_____

A Thesis

Presented to

The Faculty of the Department of Biological Sciences

Sam Houston State University

_____

In Partial Fulfillment

of the Requirements for the Degree of

Master of Science

_____

by

Nicholas Theodore Holovacs

August, 2018

MORPHOLOGICAL ADAPTATIONS OF THE SAND-SWIMMER LIZARD

CALYPTOMMATUS LEIOLEPIS (SQUAMATA: GYMNOPHTHALMIDAE)

by

Nicholas Theodore Holovacs

_____

APPROVED:

Juan D. Daza, PhD
Thesis Director

Sibyl R. Bucheli, PhD
Committee Member

Monte L. Thies, PhD
Committee Member

John Pascarella, PhD
Dean, College of Science and Engineering Technology

ABSTRACT

Holovacs, Nicholas Theodore, *Morphological adaptations of the sand-swimmer lizard Calyptommatus leiolepis (Squamata: Gymnophthalmidae).* Master of Science (Biology), August, 2018, Sam Houston State University, Huntsville, Texas.

Squamates exhibit a vast diversity of body plans. These body plans are directly affected by the habitat and how they interact within it. A common occurrence within this group is the reduction of hind and forelimbs as well as body elongation. In this study, the axial and appendicular skeleton of the fossorial gymnophthalmid, *Calyptommatus leiolepis*, is analyzed to determine how its mode of locomotion affects its osteology. *C. leiolepis* is a fossorial sand swimmer with a moderately elongated body and a short tail. With this locomotor specialty it is important to determine the specific features that result. Current descriptions of closely related species indicate that there is a level of detail that is still required. Using high-resolution computer tomography (HRCT) each bone element within the skeleton was digitally segmented and a detailed description rendered. Key features related to the fossorial sand swimming nature of *C. leiolepis* include the head exhibiting a wide array of adaptations such as a shovel-like snout with a well-developed horizontal cartilaginous rim, nasal cartilages that produce a sand-guard to protect the nostrils, reduced eyes covered by a brille, lack of forelimbs, extreme reduction of hindlimbs, and imbricated scales among others. In addition to the autapomorphic features of *Calyptomatus* such as the cartilaginous labial rim, a triradiated jugal (with digit-like projections), a reduced pectoral girdle with upper limb, parasternal processes that reinforce the ribcage, and a single digit in the lower limbs. When comparing this species with other gymnophtalmid lizards including fossorial species, it is clear that *Calyptomatus* exhibits the higest number of structural modifications within the family.

Despite its specialized morphology, it still retains characters that link this genus to other members of Gymnophtalmidae when included in a phylogeny based on phenotic data.

KEY WORDS: CT-scan, Morphology, Osteology, Sand-swimming, Lizard, Squamata, Gymnophthalmidae.

ACKNOWLEDGEMENTS

I want to thank all of my Committee Members, Dr. Juan Diego Daza, Dr. Monte L. Thies, and Dr. Sibyl R. Bucheli, for their support and help throughout this journey of scientific advancement. Once accepted into the Master's program here in the Department of Biological Sciences, I was lucky enough to be awarded a Teaching Assistantship. This was a tremendous help in allowing me to fund my ability to stay and complete the program. For this, I am eternally grateful to the University and especially to the Biology Department. I would like to give special thanks to my main advisor, Dr. Juan Diego Daza, for his unwavering council and for allowing me to stay with him and his loving family through the crucial graduating semester here at Sam Houston State University. It is also my pleasure to have gotten to know Maria Vallejo and Elizabeth Sullivan, fellow graduate students in my lab, who aided me in my coursework and thesis these past two years. Lastly, to the love of my life Lauren M. Sommer, who was a beacon of guidance, support, and loving affection through this trying process. You were there for me whenever I needed you and I can't wait to repay you every day of my life.

This project was funded by the Department of Biological Sciences at Sam Houston State University and the Instituto de Herpetología, Instituto Miguel Lillo, Universidad Nacional de Tucumán. Lastly, I would like to thank Ricardo "Ueso" Montero and Cecilia Guerra from the Instituto de Herpetología, Instituto Miguel Lillo, Universidad Nacional de Tucumán for access to the material within this study, and Edward Stanley from the Florida Museum of Natural History.

TABLE OF CONTENTS

Page

LIST OF FIGURES

CHAPTER I

Introduction

The Order Squamata (lizards and snakes), with more than 10,000 extant species recognized (Uetz et al., 2018), includes a diversity of body forms ranging from the typical saurian form with well-developed limbs to the elongated limbless form of snakes (Bradley et al., 2008; Vitt and Caldwell, 2008). Although the latter group constitutes 35% (3691 extant species) of the total number of squamate species, the percentage of snake-like squamates is much higher since body elongation and reduction of limbs has appeared in several extant groups, including dibamids (*Anelytropsis*, *Dibamus*), gekkotans (pygopods), skinks (e.g., *Chalcides*), cordylids (e.g. *Chamaesaura*), gymnophtalmidae (e.g., *Bachia, Calyptommatus*, *Nothobachia*), amphisbaenians, and anguids (e.g., *Ophisaurus*, *Ophiodes*) (Gans, 1975; Rodrigues, 1991; Lee, 1998; Wiens and Slingluff, 2001; Kearney and Stuart, 2004; Conrad, 2008; Zaher et al., 2009).

Elongation of the body and reduction of limbs have been reported to be highly correlated (Wiens et al., 2006) and guided by a common developmental mechanism (Greene and Cundall, 2000; Wiens and Slingluff, 2001). However, this association has been refuted and its occurrence explained as the result of constraints imposed by mechanics of locomotion and/or common patterns of environmental selection, yet involving changes in quite separated, dissociated developmental mechanisms in each lineage (Sanger and Gibson-Brown, 2004; see also Wiens, 2004). The independence of these two traits is consistent with the observed different patterns of body elongation and limb reduction in squamates (Bradley et al., 2008). It also explains cases where limb

reduction occurs whether the body is elongated or not, or the contrasting condition of fully limbed elongated body forms (e.g., some species in the skink genus *Lygosoma*).

Most limb-reduced squamates fit in two ecomorphs, a long-tailed surface dweller or a short-tailed burrowing ecomorph (Wiens et al., 2006; Bradley et al., 2008). Among gymnophtalmids that show limb reduction, two patterns have been identified: 1) forelimbs greater in size than the hindlimbs and with a very long tail (e.g., *Bachia*), and 2) forelimbs missing and hindlimbs reduced, and with a short tail (e.g., *Calyptommatus*) (Rodrigues, 1991; Pellegrino et al., 2001; Jerez et al., 2010).

Calyptommatus leiolepis (Figure 1) has reduced limbs and a short-intermediate tail, and differs from other limbless lizards in not having an extreme elongated snake-like body. This combination of traits might presuppose a limitation in locomotion, but this body form allows the species to sand swim in the loose sandy habitats of the inner dunes of the São Francisco River, Bahia, Brazil (Rodrigues, 1991; Lambertz, 2010; Siedchlag et al., 2010). In addition to reduction of limbs, this species has developed other adaptations for underground dwelling such as the development of a head with a transverse “shovel-like” snout, fusion of the head scales, eyes covered by a brille, absence of tympanic membrane, and a compressed body (Roscito and Rodrigues, 2010).

The phylogenetic placement of *Calyptommatus leiolepis* has been determined using molecular data (Pellegrino et al. 2001; Pyron et al. 2013). Based on nuclear (c-mos and 18S rDNA) and mitochondrial (12S ribosomal subunit, 16S ribosomal subunit, and ND4 protein coding regions) partitions, *C. leiolepis* was found to be nested with other species in the same genus (*C. nicterus* and *C. sinebrachiatus*). To date, *Calyptommatus leiolepis* has not been incorporated in any morphological phylogenetic analysis. Roscito

and Rodrigues (2010) described the cranial osteology of *C. nicterus* together with *Scriptosaura catimbau* and *Nothobachia ablephara.* The simultaneous description of three similarly fossorial lizards is advantageous because it allows us to focus on the particular variation of each species and avoid redundancy. It is also helpful to identify a general pattern that could be attributed to fossorial mode of life. For this reason, a re-description of the cranial anatomy of the genus *Calyptommatus* is unnecessary at this point. Instead I will be referring to those aspects not mentioned in their description, indicating only characters that might have some phylogenetic value. For a more generalized description of the genus *Calyptommatus* I refer the reader to the paper by Roscito and Rodrigues (2010). In this project new details are provided about the internal anatomy of the skull based on High-Resolution X-ray Computed Tomography (HRCT). Finally, I will be contrasting the species studied herein with available descriptions of other squamates that have similar life modes. I also test the phylogenetic position using morphology of this highly derived fossorial lizard within the framework of Squamata.

Materials and Methods

Specimens of *Calyptommatus leiolepis* were acquired from Dr. Hussam Zaher from the University of São Paulo, São Paulo, and made available by Dr. Ricardo Montero, from the Instituto de Herpetología, Instituto Miguel Lillo, Universidad Nacional de Tucumán. Six ethanol preserved specimens were prepared using different techniques, including clearing and staining, skeletonization, and HRCT to aid in the resolution of our findings with intraspecific variation in mind (Figure 2). HRCT images were obtained from the AMNH using a GE Phoenix v|tome|x s240 syste2m by Dr. Edward Stanley, with a molybdenum target and modification of the current and voltage to

maximize the range of densities recorded. Image stacks were used to create three-dimensional models of the entire animal skeleton. This imaging technology is non-invasive and allows a comprehensive look at the osteological and soft tissue anatomy without harming the integrity of the specimen. Using the computer software Avizo Lite v. 9.4 (Thermo Scientific™, Waltham, Massachusetts), the image stack consisting of 8-bit TIFF files were loaded into the program to segment individual bones. I specified the voxel values for X, Y, and Z (0.02156461μm) to determine the exact size of the specimen. Each bone of the skull, selected vertebrae to indicate regional variation, and appendicular skeleton were digitally segmented. Each bone was rendered using the volume rendering option in Avizo Lite 9.4.

Two specimens (MZUPS71139 and MZUPS71156) of *Calyptommatus leiolepis* were cleared and double stained using Alizarin red for bone and Alician blue for cartilage using the protocol of Maisano (2008). Each of the staining reagents were gradually increased in concentration until cartilage or bone, depending on the reagent, were clearly visible through the flesh. A specimen of *C. leiolepis* was formalin-fixed to avoid tissue and bone becoming disarticulated during the staining protocol. After fixation, the specimen was dehydrated in 95–100% ethanol for two days. Alcian blue powder combined with 30% glacial acetic acid and 70% ethanol was used to stain cartilaginous elements. After the cartilage was stained, the specimen was neutralized in a sodium borate solution to halt the staining process. The specimen was then placed in a saturated pancreatin solution (65% distilled water/35% saturated sodium borate) for enzymatic digestion. Once tissue became translucent, bone elements were stained using 0.75% potassium hydroxide solution with Alizarin red powder. The final clearing step required

two solutions: 30% glycerol/70% KOH and 60% glycerol/40% KOH. After clearing was completed, the stained and cleared specimen of *C. leiolepis* was stored in 99% glycerol, with the addition of thymol to prevent the growth of fungus. Both specimens of *C. leiolepis* (MZUPS71139 and MZUPS71156) were then photographed using a NIXON E4300 camera. The skull of one cleared and stained specimen was illustrated by tracing most of the bones in Adobe Illustrator (Adobe Creative Cloud Illustrator CC, 2018). The illustration represents overlapped bone sutures with dashed lines, bone colored as white, and cartilage as blue (Figure 3).

To test the phylogenetic position of *C. leiolepis*, morphological data for this species were fitted into a large morphological dataset of squamate reptiles (Gauthier et al., 2012). This data set included 193 taxa and 610 characters that were composed of both cranial and post-cranial osteology as well as a number of soft anatomy characters. Cranial characters were scored using my observations made from the HRCT scans, cleared and stained specimens, ethanol-preserve specimens, and skeletonized specimens. Each character was coded quantitatively in a binary or multi-state manner. Morphological characters were coded using the data management and processing software, Mesquite v. 3.40 (Madison and Madison, 2018). After characters were coded in Mesquite v. 3.40, the file was exported in TNT format. Characters were ordered as in Gauthier et al. (2012). The main goal of this analysis was to determine if the morphology of a very derived squamate still supports its placement within the gymnophtalmid lizards, or if this taxon would be lumped together with the so called “fossorial group” identified by Gauthier et al. (2012) that includes dibamids, amphisbaenians, and snakes, but excludes limbless gekkotans (i.e., pygopods). Due to large variation in morphology within the

gymnothalmids, it is worthwhile to determine if there is a conflict in the placement of *C. leiolepis*. The optimality criterion of maximum parsimony was used to provide a measure of confidence for the analysis, which was performed in TNT v. 1.5 (Goloboff and Catalano, 2016). Phylogenetic analysis used new technology options which includes a combination of sectorial search (RSS, CSS, 3 changes in sectors of size below 75, and 10 changes in sectors of size above 75) and tree fusing (3 rounds, swap after exchanging, start from best tree, and use fusing to multiply optimal trees). The outgroup taxa used in my analysis was *Sphenodon punctatus*. After the search was completed, a strict consensus tree was calculated and Relative Bremer, Bremer, and Bootstrap support were used as measures of node support. Common synapomorphies for each node were indicated for relevant nodes.

Figure 1. Whole specimen of *Calyptommatus leiolepis* (MZUSP 71139).

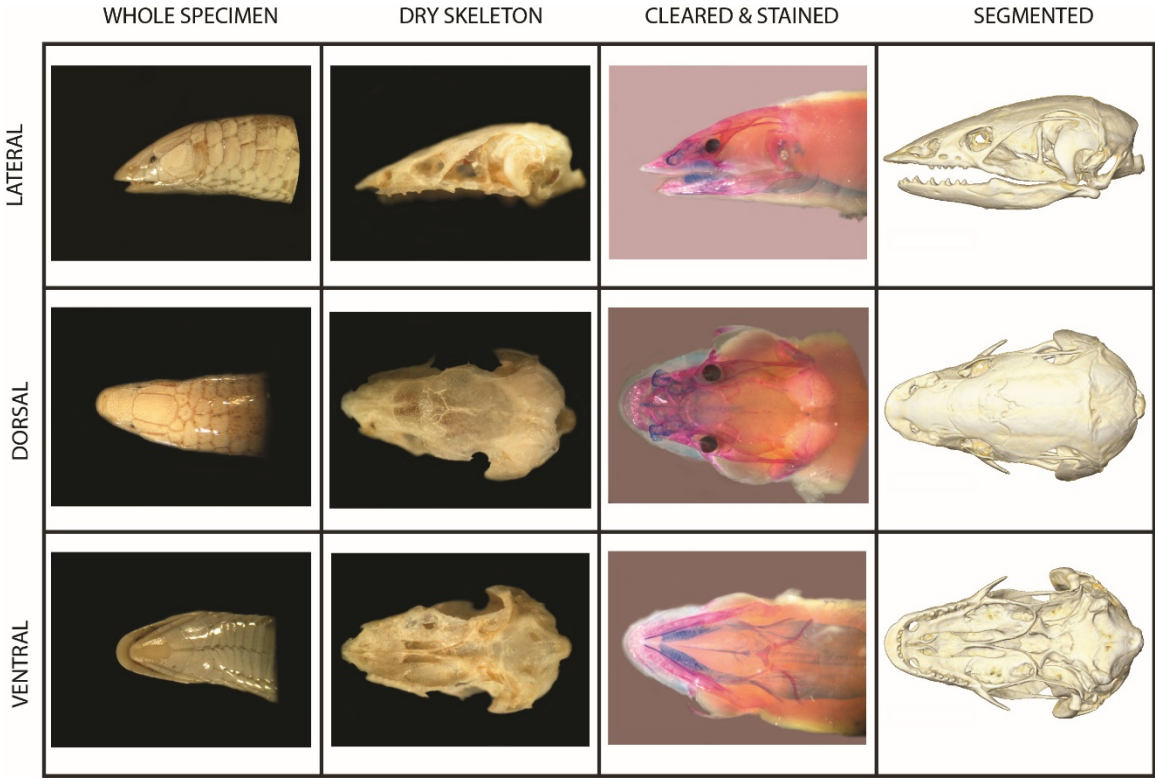

Figure 2. Lateral, dorsal, and ventral views of four preparations *of Calyptommatus leiolepis* specimens: whole body dissection (MZUSP 71147), dried skeleton (MZUSP 71367), cleared and stained (MZUSP 71156), and HRCT segmentation (MZUSP 71156).

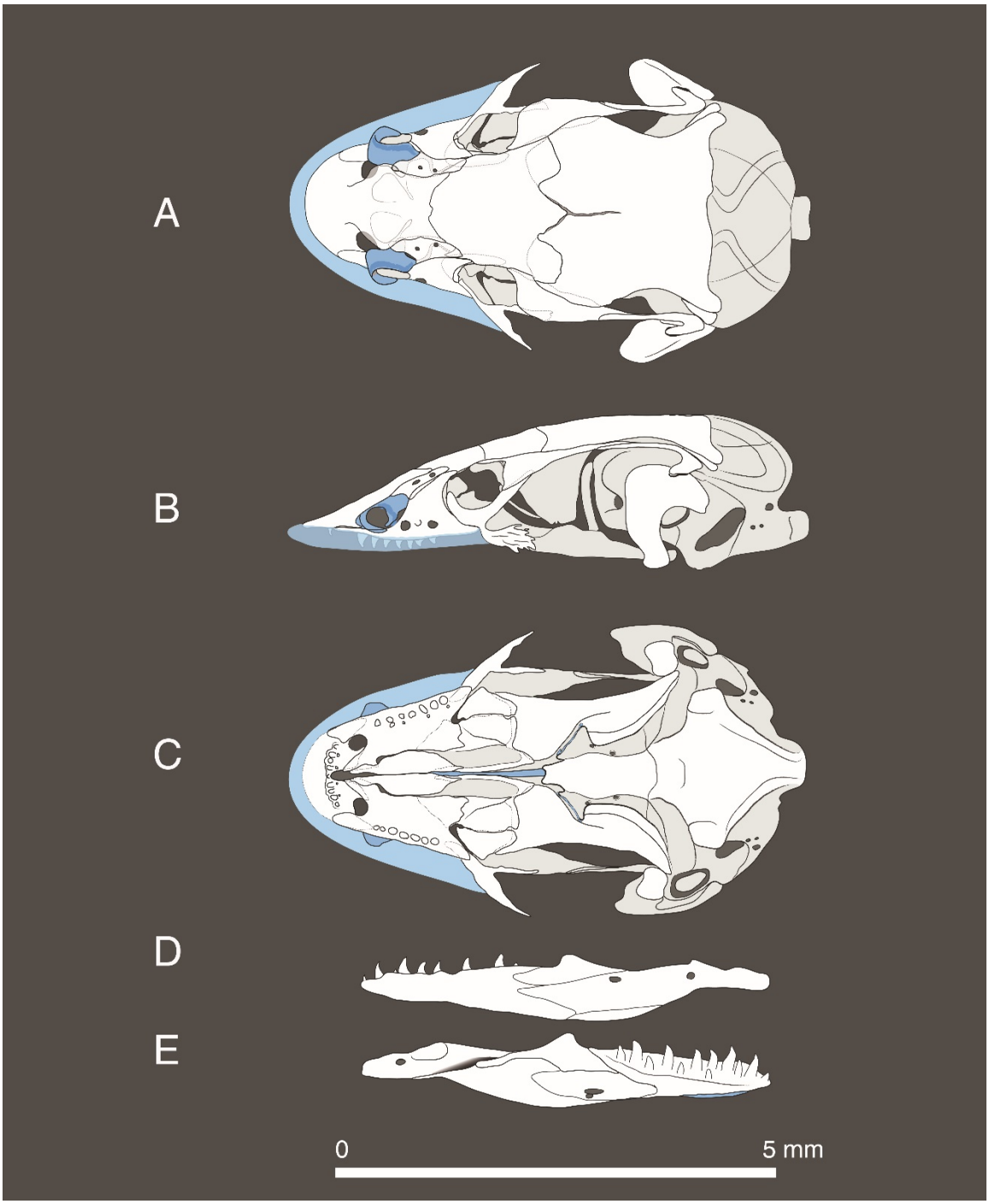

Figure 3. Illustration of the cranium of *Calyptommatus leiolepis* in dorsal (A), lateral (B), and ventral (C) views; and the left jaw in lateral (D) and medial (E) views. Dashed lines represent the overlapping of bone, white/light grey color is bone, and blue color is cartilage.

CHAPTER II

Results

The skull of *Calyptommatus leiolepis* is small (MZUSP 71156 ~ 6.8 mm in length), longer than wide, with a snout that is rounded and depressed (Figures 3A–C). The skull is somewhat oblong, caused by a cartilaginous rim that is attached to the premaxilla, maxilla and jugal (Figures 4 and 5). This creates a lateral and flattened extension of the snout with a lip that produces the impression of an overbite (Figure 4). The anterorbital snout is shortened, and the external nares open laterally. These openings bear external cartilaginous nasal flaps similar to car fenders that are upward and forward external projections of the nasal cavity that seemingly help to prevent loose soil from entering the nasal passages (Figure 5).

The eye socket is small and complete posteriorly and is surrounded by the circumorbital bones, prefontal, jugal, postorbitofrontal, and participation of the maxilla and frontal bones (Figure 6A). The eye socket, having a diameter that is about 11% of the total skull length, opens almost dorsally, giving the impression that the animal is looking upward. The frontoparietal suture is located about midway along the length of the skull length (Figure 6B). This species, as in many other gymnophtalmids, has reduced kinesis in the palate and the mesokinetic plane because the development of the paired tabs forms an interlocking frontoparietal suture (Arnold, 1998; Bell et al., 2003; Evans, 2008) (Figure 6B, C). In *C. leiolepis* there is an additional posteromedial process of the frontal that invades the interparietal suture (Figures 6B; 8R, 8S). The basicranium is proportionally large as in miniaturized lizards, especially in the area occupied by the otic

capsules (Rieppel, 1984a) as well as the posterior portion being globular and not covered by the parietals (Figure 6A–C).

The skull appears wedge-shaped and compact in lateral view (Figure 6A). Posterior to the postorbital bar, there is a wide infratemporal opening and a much smaller supratemporal fenestra, but neither is reduced or closed as is common in miniaturized specimens (M. C. Vallejo personal communication).

In ventral view, an oval and elongated premaxilla-vomer fenestra is visible (Figure 6C). The tooth arcade develops a well-defined gap or diastema, which is formed by a short portion of the premaxilla (approximately one tooth locus of space) and an anterior toothless portion of the maxilla (Figure 6C). The formation of this diastema is possibly due to the extensive suture overlap between the premaxilla and maxilla. There is also a circular premaxillary-maxillary aperture between these two bones (Figure 6C). The fenestra vomeronasalis is very small and notably shifted medially as consequence of the greater development of the maxillary palatal shelf, this fenestra is almost separated from the fenestra exochoanalis, which is almost closed, but the vomer and maxilla fail to abut or overlap; therefore, this species stills presents the paleochoanate condition (Lakjer, 1927; Rieppel et al., 2008). The palate is duplicated, with a very deep choanal groove along the palatine and that forms a secondary palate partially covered by bone and cartilage. The suborbital fenestra is very small (almost closed) and irregular in shape (Figure 6C). The interpterygoid vacuity is also greatly reduced by the anterior extension of the parasphenoid and the closeness of the palatines: this space is almost limited to a narrow slit occupied by the cartilaginous cultriformis process. The posterior process of the pterygoid also develops medial plates that form a floor for the recesus vena jugularis.

The pterygoid is very rigid, indicating the reduced mobility of the palate, although the joint with the basipterygoid processes is still cartilaginous. This indicates the presence of a synovial joint with the braincase.

Individual bone descriptions

The Mandible

The mandible is comprised of five bone elements: the dentary, coronoid, splenial, angular, surangular, and compound bones (Figure 7C–F). Overall, the posterior portion of the jaw exhibits signs of fusion that obscure the distinct suture lines for individual bones.

The dentary extends posteriorly, coming in contact with the angular ventrally via the superior and inferior processes (Figure 7C, D, F). The superior process extends to about the posterior edge of the coronoid while the inferior process stops at the anterior portion of the external mandibular fenestra (Figure 7C, F). This bone is concave, curving medially, containing three mental foramina within the anterior one-third of the lateral surface (Figure 7C). Each dentary contains approximately 10 pleurodont teeth that are well spaced and recurved with somewhat expanded bases (Figure 7C, D, F). The dentition resembles that of certain groups of Amphisbaenidae, Pygopodidae, Anguidae, Helodermatidae, and Varanidae that contain recurved teeth that come to sharp terminal points (Hoffstetter and Gasc, 1969).

The splenial contains two foramina that are visible on the medial surface, the alveolar foramen and anterior mylohyoid foramen (Figure 7F). These foramina are found ventral to the anteromedial process of the coronoid (Figure 7F).

The angular is small and in a posterior position within the jaw, making contact with the compound bone posteriorly, splenial anteriorly, and surangular dorsally. The

posterior mylohyoid foramen is positioned anteroventrally, almost making contact with the surangular posteromedially (Figure 7E–F). On the lateral face of the surangular the large surangular foramen comes in contact with the coronoid ventrally, below with the posteromedial process, and is in close contact posteriorly with the posterodorsal process of the dentary (Figure 7C). The compound bone (prearticular-articular bone) extends posteriorly from the coronoid and dentary (Figure 7C–F). Between the retroarticular process and posterior part of the surangular is a concave fossa where the quadrate articulates (Figure 7D). The articulation occurs in between the lateral and medial condyles of the quadrate.

Premaxilla

The nasal process of the premaxilla contacts the nasals laterally, the frontal posterodorsally, and the vomer posteroventrally (Figures 6B, 7A). This bone is wide and long, presents a complex shape, and is the most prominent element of the snout (Figure 8A–E). It forms the dorsolateral border of the naris, roofing the most part of the nasal cavity and the septomaxilla. This bone bears nine teeth that are attached towards the posterior edge of the palatal shelf (Figures 6C; 8 B, E). As consequence of not being attached to the margin of the tooth arcade, the tooth implantation is pleurodont, but the medial wall of the premaxillary parapet is very low, and it renders a view that makes tooth implantation almost acrodont. The premaxilla contacts the maxillary lappets, and the anterior processes of the vomer separates the maxillae, and contacts briefly the premaxilla. The premaxilla palatal shelf is indented and forms the anterior margin of the premaxillary-vomer fenestra (Figure 6C). Nested within the lateral process of the premaxilla is a notch into which the anterior process of the maxilla inserts (Figure 8A–E).

Maxilla

This bone has a tall facial process with a steep incline behind the nares (Figure 8F–J). This process is concave posteriorly, forming part of the margin of the eye socket (Figure 6A). The facial process is located on the posterior portion of the bone and is pierced by two to three large vascular foramina through which presumably the terminal branches of the maxillary artery and the maxillary branch of cranial nerve V exit to the nasal capsule (Figures 6A, 8F) (Oelrich, 1956; Evans, 2008). This bone together with the frontal entirely overlap the prefrontal; therefore, it is not visible dorsally (Figure 6 A–B). The palatal shelf is very broad and almost rectangular in shape (Figure 8J). It bears six pleurodont teeth, the same number as in *C. nicterus* (Figures 6C, 8J) (Roscito and Rodrigues, 2010). Some of the maxillary teeth are almost twice the size of premaxillary teeth (Figure 6C). The palatal shelf forms the posterior margin of the premaxilla-maxilla aperture, participates briefly in the premaxillary-vomer fenestra, forms the anterior margin of the fenestra vomeronasalis, the lateral margin of the fenestra exochoanalis, and the anterior margin the suborbital fenestra (Figure 6C). Specifically, the anteromedial and anterior process aid in the creation of the posterior margin of the premaxilla-maxilla aperture (Figures 6C, 8I–J). In addition, the posteromedial and posterior process of the maxillary shelf come in contact with the palatine and ectopterygoid, respectively (Figures 6C, 8I–J). The osseous naris edge is concave, abutting against the nasal and aiding in the formation of the posterior edge of the naris (Figures 6A–B, 8F–J).

Nasal

This bone is very membranous and subtriangular in shape, with a concave anterior margin and a blunt posterior margin (Figures 6A–B, 8G–H). It forms the dorsal wall of

the nasal capsule. This bone has extensive, slightly overlapping contact with the premaxilla (medially) via the premaxilla facet, and the maxilla (laterally) via the maxilla facet (Figures 6B, 8G–H). It also overlaps the anterolateral process of the frontal bone and a small part of the prefrontal. The nasal bones bear from 1 to 3 vascular foramina, which in some specimens may be asymmetrical. The osseous naris edge aids in the posterodorsal margin of the external nares (Figures 6A, 8G–H).

Prefrontal

In *C. leiolepis*, this bone is almost completely concealed by the facial processes of the maxilla and the jugal (Figure 6A–B). This bone has a dorsal process that extends posteriorly beneath the frontal bone: it forms most of the inner anterodorsal wall of the orbit while the anterodorsal orbital rim is formed mostly by the maxilla and the frontal (Figures 6A–B, 8K–N). The prefrontal contacts the nasal ventrally but in lateral view the terminus of the facial process of the maxilla separates the prefrontal from the nasal (Figure 6A). In *C. nicterus* (Roscito and Rodrigues, 2010**)** the prefrontal is not visible in dorsal view, while in *C. leiolepis* this bone is slightly visible (Figure 6B).

Postorbitofrontal

The only element on the posterodorsal border of the orbit in *Calyptommatus* is formed by the fusion of the postfrontal and the postorbital (Figures 6A–B, 8O–P) (Roscito and Rodrigues, 2010). The squamosal makes contact with this bone on the dorsal edge via the squamosal facet (Figures 6A–B, 8O–P). Some specimens present a small foramen in this bone, which supports observations by Roscito and Rodrigues (2010) and the argument that the postfrontal and postorbital are fused in pygopodids (Rieppel, 1984b). This bone is wide and tapers posteriorly where it contacts the

squamosal to form the upper temporal bar. This bone forms the posterodorsal portion of the orbit (with the aid of the anterior process, lateroventral process, and the ridge that connects the two) and clasps the frontoparietal suture (Figures 6A, 8O–P).

Jugal

The jugal bone is curved and has a triradiate shape as in *C. nicterus*, which appears to be a synapomorphy of the genus. It is formed by a dorsal postorbitofrontal process that contribute to the postorbital bar, an anterior maxillary process, and a posterolateral process (Figures 6A–C, 8Q). The posterolateral process is expanded posteriorly and in some specimens may present digit-like posterior projections and some sculpturing (Figures 6A, 7Q). The posterolateral process has a dual function, serving for the anterior attachment site of the cartilaginous rim to the snout, and posteriorly for the ligamentous rictal plate that links the jugal with the anterior margin of the quadrate (Figure 5).

Frontal

This bone is crown shaped, having an anterior end that is half the width of the posterior end. *Calyptommatus* does not present the inter-orbital constriction seen in other gymnophatalmid genera, but it resembles other fossorial forms where the frontal tends to have parallel margins. In *C. leiolepis* there is a posteromedial process that invades and separates the parietals anteriorly (Figures 3A, 6B, 8R–S): this process is not present in *C. nicterus*, which presents a straight medial margin. This bone also exhibits parietal tabs in the posterior region that aid in forming a robust support structure (Figures 6B, 8R–S). The frontal participates in forming the orbitonasal fenestra along with the palatine and the prefrontal. It also contains laminar descending processes (crista cranii) that contact the

orbitonasals anteriorly and laterally protect the olfactory tracts without joining ventrally (Figure 8R–S).

Parietal

This bone in *C. leiolepis* remains unfused in the anterior portion, the position of the parietal fontanelle: in *C. nicterus* it is completely fused. Another difference among these species is the major development of a medial constriction in *C. leiolepis*, which leaves the prootic portion of the braincase exposed in dorsal view. The postparietal process is more rounded than in *C. nicterus* (Figures 6B, 9A–C). The significant development of a decensus parietalis process in the genus *Calyptommatus* contributes to the anterolateral closure of the braincase with the epipterygoid and orbitosphenoids (Figures 6A, 9B–C). This laminar process has a nearly rectangular shape with more or less straight ventral margin, and remains separated from the pterygoid, epipterygoid and orbitosphenoids (Figure 6A). The frontal overlaps this bone on the frontal facet, located on the anterior end of the parietal dorsal to the decensus parietalis process (Figure 9A–B).

Supratemporal

This is a small splint of bone inserted between the postparietal process of the parietal and the squamosal (Figures 6A, 9D). In *C. leiolepis* it is in contact with the either the cephalic condyle of the quadrate or the paroccipital process of the otooccipital posteriorly as in *C. nicterus*, where this bone seems to be more vertically oriented. This orientation positions the dorsal process in between the parietal and the start of the squamosal shaft (Figures 6A, 9D).

Epipterygoid

This is a columnar bone that lies between the prootic and the decensus parietalis process of the parietal (Figure 6A). It contributes to the closure of the braincase laterally and is inserted in the fossa columella of the pterygoid. The bone is compressed and resembles a knife (Figures 6A, 9E).

Squamosal

The bone has the typical hockey stick shape of lizards (Figures 6A, 9F–G) (Robinson, 1967; Rieppel, 1994). The shaft is curved and has a long overlapping suture with the postorbitofrontal (Figure 6A). It defines the lateral margin of the supratemporal fenestra (Figure 6A). The posterior process is lateroventrally expanded and contacts the dorsal surface of the quadrate (Figure 6A).

Vomer

This bone is elongated in *C. leiolepis* and is not entirely fused in adults. The paired vomers remain separated anteriorly and posteriorly, in the former producing a posterior expansion for the premaxilla-vomer fenestra and the later an anterior expansion of the interpterygoid vacuity (Figures 6C, 9H–I). The vomer also forms the posteromedial margin of the fenestra vomeronasalis, the medial margin of the fenestra exochoanalis, and participates in the choana. The anterior processes of the vomer are continued posterolateraly into two conspicuous ventral crests (Figure 9I). In dorsal view, the anterior process show two short anterolateral processes, which together with two transverse ridges define the area occupied by the vomeronasal organ (Figure 9H). In ventral view, the vomer is overlapped by the palatine on the posteriorly located palatine process (Figure 6C).

Palatine

This bone is nearly rectangular in shape and overlaps the posteromedial portion of vomer and a large triangular area that correspond to the posteromedial flange of the maxilla (Figure 6C). Posteriorly this bone is overlapped by the pterygoid, and slightly by the ectopterygoid (Figure 6C). The palatine is extremely furrowed, forming a duplicated palate that is partially covered by a cartilaginous sheet that forms an incomplete secondary palate. In the HRCT model, the palatine bone was rendered in combination with the pterygoid and ectopterygoid because the resolution of the scan did not allow these bones to be separated; however, in the cleared and stained specimen, it was evident that they are not fused but clumped together (Figures 6C, 9J–L). The palatine forms the posteromedial border of the suborbital fenestra (Figure 6C).

Ectopterygoid

This bone is triangular shaped, flattened, and broad (Figure 9J–L). It does not contact the maxilla anteriorly, but has extensive contact with the maxilla medially and with the pterygoid posteriorly (Figure 9J–L). In *Calyptommatus* this bone becomes enlarged, and as a consequence the suborbital fenestra becomes extremely reduced (Figure 6C) (Roscito and Rodrigues, 2010). This bone forms the posterolateral border of the suborbital fenestra (Figure 6C).

Pterygoid

This is the longest bone of the cranium. In *C. leiolepis* it is excluded from the suborbital fenestra by the extensive contact between the palatine and the ectopterygoid (Figures 6C, 9J–L). The bone bears on its dorsal surface the fossa columella where the epipterygid inserts (Figure 9J). The pterygoid participates in the synovial joint with the

braincase. Posterior to this articulation, the bone develops two inward blade-like structures that cover ventrally the lateral margins of the braincase (Figure 6C). Contrary to *C. nicterus* (Roscito and Rodrigues, 2010), in *C. leiolepis* the pterygoid has two discrete anterior processes, a pointed lateral process that bounds the ectopterygoid posteriorly, and a broad and nearly transverse medial process (with a minimal projection) that contacts extensively the palatine (Figures 6C, 9J–L). In the posterior region of the pterygoid a laterally pointed quadrate process with a quadrate facet that abuts the quadrate for articulation with the jaw (Figure 6C).

Quadrate

This bone is suspended from the squamosal, supratemporal and the paroccipital process (Figure 6A–C). The mandibular articulation is bicondylar: the lateral condyle is slightly larger than the medial one (Figure9 M–P). The anterior, lateral, and medial surfaces of the quadrate are convex and the posteroventral is slightly concave (Figure 9M–P). The posterior concavity defines a reduced middle ear space which is mostly filled by the columella auris and some small ossifications. Between the posterior crest and central pillar there is a large cavity that extends within the body of the quadrate (Figure 9M, P). On the ventral region, dorsal to the medial condyle, there is a pterygoid facet in which the pterygoid abuts for mandibular articulation (Figure 9M, P).

Otostapes

This bone is highly modified having a rivet shape, consisting of a broad footplate joined by a very short and subtriangular shaft (Figure 10C). The footplate fits tightly into the fenestra ovalis (Figures 6A, 10C). Its shaft is very short and is expanded laterally

from where a thin and wing-like extrastapes originates (Figures 6A, 9Q–S, 10B–C). These two structures combine to form the columella auris.

Sclerotic Ring

The ossicles within this ring structure of the orbit are reduced and completely fused creating a cone-like appearance (Figures 6A–B and 9T–U). Additionally, the sclerotic ring is narrow and steeply angled, as if pointing laterally out of the orbit (Figure 6A–B). This morphology mirrors all other squamate groups that are also fossorial and have not completely lost the development of the sclerotic ring (Atkins and Franz-Odendaal, 2016).

Neurocranium

In *C. leiolepis* the sutures are easy to identify. Compared to *C. nicterus* this species has a more globular braincase. In general, these two species present similar suturing in the braincase. The main difference in suturing between the two species is the presence of a large parietal fontanelle (Figures 6B, 7A, 9A–B).

Orbitosphenoid

The paired orbitosphenoids are small and slender bones that are anteriorly placed in the braincase, just in front of the decensus parietalis process of the parietal. These two bones are articulated medially in front of the braincase.

Prootic

The crista alaris is absent and this creates a rectangular outline when viewed laterally (Figure 10C). This anterior part of the basicranium contacts only the epipterygoid, which lies between the braincase and the decensus parietalis process (Figure 6A). Anterior to the prootic, there is a downward projecting process that includes

the incisura protica. In *Calyptommatus* the incisura prootica is entirely closed and pierces the prootic, so instead of being a notch it is a foramen (Figure 10C–F). The same foramen is developed convergently in nearly all gekkotans, and in that group is called the foramen prootico (Daza et al., 2013). Additionally, the incisura prootica is the course for the trigeminal nerve (cranial nerve V). Roscito and Rodrigues (2010) describe the presence of a crista prootica, but they did not specify in which three burrowing taxa it was present. In *Calyptommatus* the crista prootica is poorly developed, and below it, there is a limited space for the recesus vena jugularis, which is partially covered by a medial laminar projection of the pterygoid (Figure 10A–D). The facial foramen opens laterally, posterior to the foramen prootico, and just anterior to the fenestra ovalis (Figure 10C). The prootic forms the anterior half of the fenestra ovalis (Figure 10A–F).

Otooccipital

This bone forms the posterolateral side of the cranium (Figures 6A, C; 10A–F). It forms the posterior half of the fenestra ovalis, and the anterodorsally oriented fenestra rotunda (which is oval instead of rounded) (Figure 6A, C). The fenestra rotunda in lizards is also termed the lateral opening of the recessus scalae tympani (LARST; Rieppel, 1985). The LARST in *Calyptommatus* is located posterior to the fenestra rotunda, this seems to be shared also with *Scriptosaura*, while in other squamates LARST is usually located below the fenestra rotunda (Figures 6A, 10C, D).

The fenestra ovalis and the LARST are separated by the crista interfenestralis, which narrows ventrally and expands dorsally toward the paroccipital process (Figure 10C). The paroccipital process is very reduced and located dorsally from the otostapes (Figure 10C). The crista tuberalis is very faint, and originates posteriorly, curving around

the posterior border of the fenestra rotunda (Figure 10C). The crista tuberalis projects ventrally towards the ventrally directed sphenoccipital tubercle where it is capped by a distinct ossification, the basicranial sesamoid (Figures 10B–F, 11) (Montero et al., 2017). Posterior to the crista tuberalis there is a well-defined vagus foramen, which marks the division between the two elements that compose the otooccipital, the opisthotic and exoccipital (Figure 10C) (Bever et al., 2005). Below the vagus foramen are two hypoglossal nerve foramina (Figures 6A; 10B, C, F). In *C. nicterus* and other gymnophalmids, two (Bell et al., 2003; Guerra and Montero, 2009; Roscito and Rodrigues, 2010) or three (Tarazona et al., 2008) small foramina have been described. The otooccipital forms the lateral margin for the foramen magnum and they participate in the formation of the prominent occipital condyle (Figures 3A–C; 6A–C; 7B; 10A–D, F).

Supraoccipital

This bone forms the dorsal margin of the foramen magnum, and its posterior margin is rounded (Figures 3A–B; 6A–B; 7B; 10A, C, E, F). This bone is completely roofed by the parietal in *C. leiolepis*, and as consequence, the posttemporal fenestrae disappears; the lack of these fenestrae is a difference with *C. nicterus* where two slender openings are persistent (Figures 6B, 7B). Similarly, the process ascendens tectum synoticum in *C. leiolepis* is not developed; therefore, the parietal and the supraoccipital developed a wide suture contact (Figures 3A, 6B).

Parabasisphenoid

This bone presents medially an elongated parasphenoid rostrum, from where the cartilaginous cultriformis process originates (Figures 3C, 6C, 10A–E). The cultriformis process is a long rod that extend up to the level of the vomer (Figure 11). The

parasphenoid rostrum extends farther anteriorly than the basipterygoid process (Figures 3C, 6C). The basipterygoid processes are covered by cartilaginous pads and form a synovial joint with the medial flange of the pterygoid (Figure 11). The basisphenoid is pierced by the abducens canal and the Vidian/carotid canals (Oelrich, 1956; Conrad, 2004; Bever et al., 2005). In ventral view the posterior opening of the Vidian canal is visible near the base of the basipterygoid process.

Basioccipital

This bone forms the majority of the occipital condyle (Figures 3C; 6C; 7B; 10B, F). The occipital condyle protrudes posteriorly, which is a character for miniaturized species (Figures 3C; 6C; 7B; 10B, 10F; Vallejo, personal communication). The occipital condyle is nearly rhomboid and convex ventrally. In the specimens of *C. leiolepis* we did not find any contribution to the border of the LARST, but it forms the projection of the sphenoccipital tubercles (Figures 10B–F, 11).

Hyoid apparatus

The apparatus consists of a five ossified/bone elements (three paired and one unpaired) and two cartilaginous elements: basihyal, hyoid cornu, glossohyal, 1st ceratobranchial, epihyal, 2nd epibranchial, and 2nd ceratobranchial (Figure 12A–B). The basihyal is shaped like a shark tooth with the apical process pointing toward the mandibular symphysis and the two basal processes extending postero-laterally (Figure 12A–B). Extending antero-laterally from the lateral position of the basal processes of the basihyal is the hyoid cornu (Figure 12A–B). This structure extends towards the inferior process of the dentary. The glossohyal is positioned medially and is angled at about 45^{o} toward the vomer (Figure 12A–B). Positioned posteriorly of the basal processes of the

basihyal are the ceratobranchials, of which it articulates. This ossified element extends postero-laterally as well as angles dorsally pointing towards the atlas (Figure 12A–B). Posterior to the basihyal there are straight filamentous projections that follow the trachea posteriorly, extending beyond the 1st ceratobranchial (Figure 12B). Attached to the 1st ceratobranchial on the posterolateral end is a small cartilaginous element, the 1st epibranchial (Figure 12B).

Pectoral girdle

The pectoral girdle consists of a clavicle, interclavicle, suprascapular, scapulocoracoid, sternum, xiphisternum, and parasternum (Figures 13A–B, 14). The clavicle is thin and narrow, located anteriorly from the scapulocoracoid and interclavicle (Figure 13A–B). The clavicle contacts the suprascapula dorsolaterally and interclavicle posteriorly (Figure 13A–B). The interclavicle is positioned anteriorly from the sternum following the contour of the two anteromedial sternal processes (Figure 13A–B). Overall, the pectoral girdle is similar in morphology to that of *C. nicterus,* but is distinct in that it contain a larger (~4x) central foramen within the sternum, a sternum that extends further posteriorly, and a more narrow suprascapular (Roscito and Rodrigues 2012). To increase rigidity to the pectoral region, *Calyptommatus leiolepis* has developed a consolidation of the rib cage via the parasternum, which consists of a series of ventral bony ribs that overlap the adjacent structures in the same way that it does in birds (Figure 14). The presence of parasternal ribs has also been reported in other gymnophthalmids (e.g., *Bachia intermedia, C. nicterus*, *Nothobachia ablephara*, and *Scriptosaura catimbau*) and seems to be a synapomorphic trait for some groups within the Gymnophthalmidae (Camp, 1923; Roscito and Rodrigues 2013).

Pelvic girdle and limbs

The pelvic girdle contains a long hypoischium (~2mm) that extends posteromedially from the pubic tubercle (Figure 13C). On the posterolateral edge of the girdle between the ischium and pubis is a small obturator foramen (Figure 13C–D). Lateral to the obturator foramen is a small lateral pectineal process that contours the femoral condyle (Figure 13D). On the posteromedial edge of the ischium lies a poorly developed ischial tuberosity that is directed posterolaterally (Figure 13D). There is a dorsally directed epiphyseal tuberosity extending from the ilium (Figure 13E). The pelvic girdle exhibits no fusion on the medial edges of both the ischium and pubis (Figure 13C–D). The femur is the same length as the phalange, metatarsal, fibula, and tibia combined (~2.75mm) and is directed posterolaterally (Figure 13C–E). The hind limb exhibits only a single metatarsal and phalange that are roughly the same length (~0.75mm) (Figure 13C–E).

Cervical vertebrae

The cervical vertebrae exhibit a concave morphology of the neural arches, which are pointed medial at the dorsal tip (Figure 15A–E). In the middle portion of the neural arches there is a very small posterodorsal process (Figure 15A–E). Below the posterodorsal process, on the anterior side of the atlas, is a small laterally curved transverse process that connects to the occipital condyle facet (Figure 15B), which is the point of contact between the atlas and braincase for universal movement of the cranium (Figure 15B). In dorsal and lateral views, the vertebrae are tapered at the ventral end and become wider behind the posterodorsal process (Figure 15D–E). The intercentrum is

located on the ventral portion of the vertebrae and exhibit very small contact with both arches, medially from the transverse processes (Figure 15A–C).

The axis is tall, containing two prominent blade-like processes on the dorsal and ventral surfaces (Figure 15F). The dorsal neural spine is angled posteriorly with a slight anterior overhang (Figure 15F). Below the neural spine there is a small projection of the postzygopophysis that comes in contact with the succeeding vertebra's prezygopophysis (Figure 15F). The transverse process is directed posterolaterally and extends past the body of the vertebra (Figure 15G). There is a large anteriorly projected odontoid process that makes contact with the odontoid process facet of the atlas (Figure 15A). The odontoid process is wide at the base and tapers to a small anterior process (Figure 15F–G).

Thoracolumbar vertebrae and ribs

Each of the trunk vertebrae are procoelous, and contain a dorsal neural spine, anterodorsally directed prezygopophyses, posteroventrally directed postzygopophyses, and lateral synapophyses with which the tubercles of the ribs make contact with the vertebra (Figure 15H–M). The presacral vertebral series varies in neural spine length and direction, length of the centrum, and thickness of the hypapophysis (Figure 15H–M). The anterior presacral vertebrae, located in the thoracic region above the sternum, are short in centrum length (~1.2mm) and stout (Figure 15H). In lateral view, the neural spine is tall and directed slightly posteriorly (Figure 15H). On the ventral side of a presacral vertebra the hypapophysis is thin and directed ventrally slightly passed the synapophysis (Figure 15H–I). The next posteriorly located presacral vertebra has a more blunt neural spine that is directed further posteriorly as well as a more rounded hypapophysis that does not

project ventrally passed the synapophysis (Figure 15J). The next vertebra exhibits the same process of blunting of the hyapophysis and neural spine with an even more posteriorly angled neural spine (Figure 15L–M).

The ribs contact the vertebrae at the synapophyses and are present in all presacral vertebrae except for the first three cervical vertebrae (Figure 17). From anterior to posterior, the ribs extend laterally from the vertebral column and reach a maximum width at about the midpoint of the column and then constrict towards the sacrum (Figure 17).

Sacrum

This bone is formed by the fusion of two sacral vertebra, these to vertebra define two sacral foramina, one between each of the connections of the transverse process for each sacral vertebrae (Figure 16A–B). Both sacral foramina are located medially within the vertebra ~0.5mm from the midline (Figure 16A). This bone also contains two neural spines, the anterior one is shorter in length compared to the posterior one (Figure 16A–B), which is almost twice as long as the anterior one.

In fully limbed, tetrapod forms, squamates the sacrum is separated into two distinct vertebrae (Hoffstetter and Gasc, 1969). Deviation from this morphology is common with the incorporation of a vertebra anterior or posterior to the two original sacral vertebrae (Hoffstetter and Gasc, 1969). Within groups of fossorial and limb-reduced squamates, the sacral vertebrae became fused at their neural spine, centra, and distal ends of their transverse processes (Hoffstetter and Gasc, 1969). The fusion of these two vertebra are not complete, thus leaving a small foramina (sacral foramen) clearly visible on the ventral side (Figure 16A). This simplification of sacral morphology within

Calyptommatus leiolepis can be seen in other groups such as *Bachia*, *Ophiodes*, and others (Hoffstetter and Gasc, 1969; Camp 1923).

Caudal vertebrae

The caudal vertebrae have an elongated morphology (Figure 15N). The caudal vertebrae contain a more extended neural spine than in the sacral and presacral vertebrae (Figure 15F–O). On the dorsal tip of the neural spine there is a slight anteriorly positioned notch (Figure 15N). Due to the elongated nature of the caudal vertebrae, the intervertebral foramen is slightly extended to the center of the vertebra, giving it a more oval appearance (Figure 15N). The prezygopophysis is also extended anteriorly 0.5mm from the intercentrum (Figure 15N). These vertebrae contain two pairs of transverse processes that extend laterally on either side, a unique characteristic of only a few squamate groups (Ethridge, 1967; Figure 15N–O). On the anterior end of the last caudal vertebra there seems to be an autotomic septum located just prior to what would be the transverse processes, exhibiting the type 3 location of Ethridge (1967; Figure 15N–O). Overall, the caudal vertebrae change drastically in morphology from the first vertebra to the last.

Phylogenetic Analysis

A maximum parsimony analysis was carried out with the morphological dataset (Gauthier et al, 2012) of 193 taxa including unordered and ordered coded characters for *Calyptommatus leiolepis*. The analysis retained 50 hits and from the analysis and a strict consensus tree was formulated. Bremer, relative Bremer, and bootstrap support values were calculated from the strict consensus tree. The analysis revealed the position of *C. leiolepis* to be nested within the Gymnophthalmidae clade (Figure 18). For simplicity,

major clades are collapsed except for taxa within Scincomorpha (Figure 18). All major groups (Scincoidea, Teiidae, Gymnophthalmidae, and Lacertidae) retain placements that are supported with the underlying morphological dataset (Gauthier 2012). Synapomorphies that support the placement of *Calyptommatus leiolepis* within Gymnophthalmidae and are diagnostic for this taxa include characters: 2) premaxilla palatal shelf – (0) not bifid posteriorly; 7) premaxilla body anterior ethmoidal foramina exit via – (1) premaxilla notch; 21) nasal descending lamina – (0) absent; 31) nasofrontal suture shape – (0) without V-shaped nasal process into frontal midline; 65) postfrontal relative to parietal table – (0) ventrolateral; 70) postfrontal broad and flat – (0) not; 81) postorbital-ectoptergoid contact – (0) absent; 82) postorbital jugal ramus – (0) extends ventral to quadrate head; 84) postorbital contribution to posterior orbital margin – (3) 67-80%; 95) parietal post-parietal projection near midline – (0) absent; 119) maxilla firmly sutured to palatine – (0) present; 133) prefrontal-frontal suture in cross-section – (0) prefrontal arcs gently about anterolateral frontal margin along entire anteroposterior length; 143) jugal – (0) jugal broadly overlaps level of posterior maxillary tooth row; 166) supratemporal – (0) present; 169) supratemporal anterior suture with parietal shape – (0) supratemporal lies flat against supratemporal process of parietal; 182) quadrate-pterygoid overlap – (1) short overlap or small lappet; 185) quadrate height to braincase depth ratio – (1) 50-59%; 190) stapes – (0) imperforate; 191 stapedial shaft – (1) short and thick; 196) septomaxilla – (0) present; 211) vomeronasal organ and mushroom body – (0) not fully enclosed by septomaxilla and vomer; 212) vomer fusion – (1) absent; 258) pterygoid separation on midline – (2) broad at base but not as narrowly separated anteriorly; 308) crista prootica – (0) does not extend onto basipteryoid; 339) basal tubera

position – (1) anteromedial with apex at lateral juncture of sphenoid and basioccipital andterior and medial to prootic-opisthotic suture; 341) occipital condyle – (0) posterior surface of condyle straight in ventral view; 349) hypoglossal (XII) foramina exit - (0) hypoglossal foramina separated from vagus; 356) dentary anterodorsal edge of dental parapet at tip – (0) straight; 360) dentary subdental shelf/gutter development in anterior part of dentary – (2) pronounced subdental gutter; 361) dentary number of mental foramina on lateral surface – (3) three; 393) coronoid posteromedial process – (1) present ; 446) second ceratobranchials – (0) present; 499) clavicle – (0) present; 500) clavicle – (0) no notch or fenestration present; 501) clavicle – (0) rod-like; 503) distal clavicle articulation – (1) with suprascapula; 517) ischial tubercle – (0) present; 524) pelvic elements [ilium, ischium, pubis] – (1) distinct elements weakly united in non-sutural contacts; 526) hyperischial foramen – (0) absent; 527) epiphyses on long bones – (1) absent; 548) femur – (0) present; 556) fibulo-astragalar joint – (0) occupies less than half of distal end of fibula; and 583) mineralized cranial scales hinges – (0) absent. Additionally, the synapomorphies that are diagnostic for gymnophthalmids include: 134) prefrontal length relative to height – (1) short anteroposteriorly; 167) supratemporal shortens – (2) supratemporal very small; 225) vomer posterodorsal margin forms expanded hollow flange – (0) absent; 248) palatine choanal process – (0) forms an extensive concave surface dorsal to the ductus nasopharyngeus; 337) Vidian canal caudal opening – (0) within basisphenoid; 382) angular taller anteriorly closely approaching coronoid – (0) absent; 383) angular medial exposure – (2) narrow; and 460) cervical vertebrae number increase – (0) six or fewer.

Figure 4. Cleared and stained *Calyptommatus leiolepis* (MZUSP 71156) in dorsal (a), ventral (b) and left lateral (c) views emphasizing the broad and flattened snout with a cartilaginous rim, external nasal cartilaginous flaps that cover the nasal openings, cartilaginous jugal attachments,and the basicranial sesamoids for insertion of the longus coli muscle.

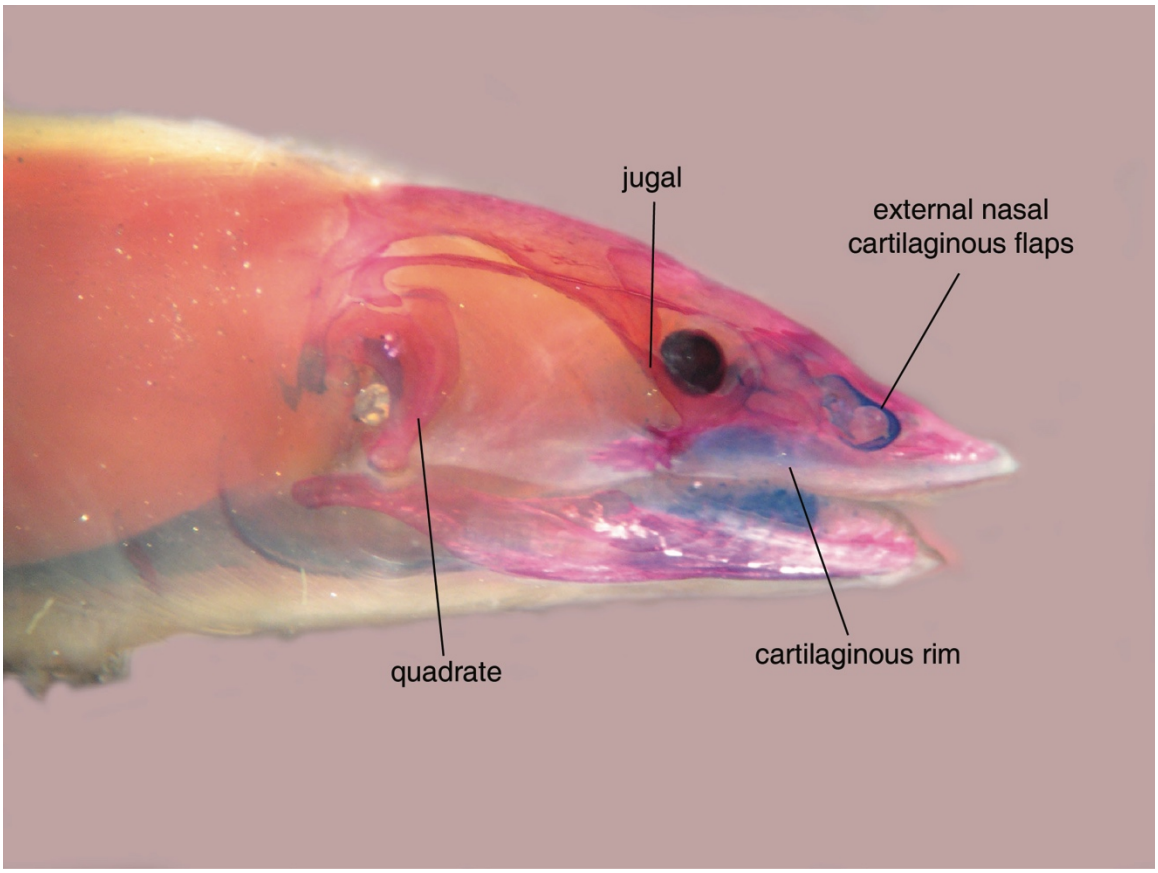

Figure 5. Cleared and stained *Calyptommatus leiolepis* (MZUSP 71156) in lateral view emphasizing the external nasal cartilaginous flaps that cover the nasal opeinings and cartilaginous jugal attachments.

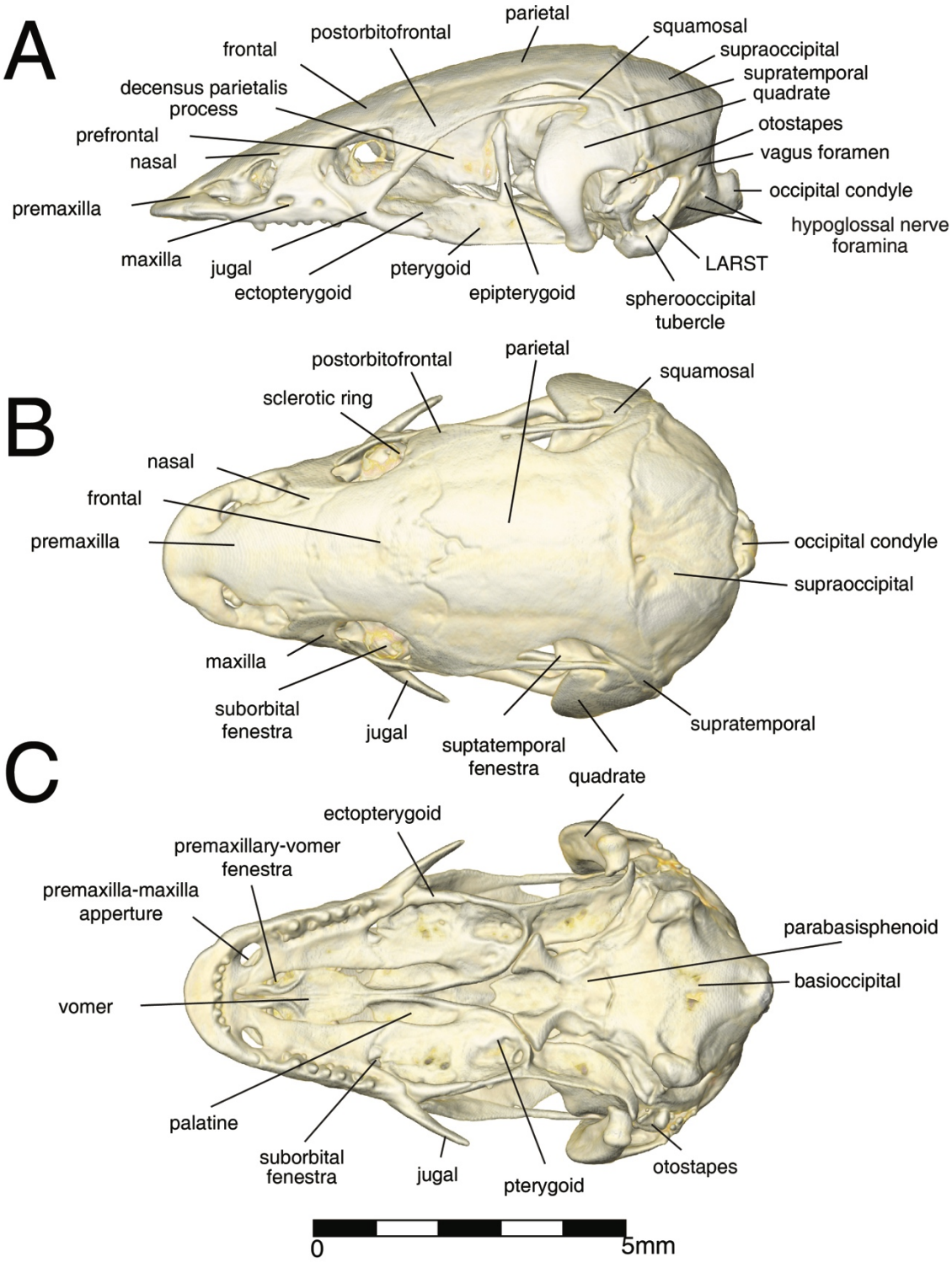

Figure 6. The cranium of *Calyptommatus leiolepis* (MZUSP 71156). Skull in (A) lateral, (B) dorsal, and (C) ventral view.

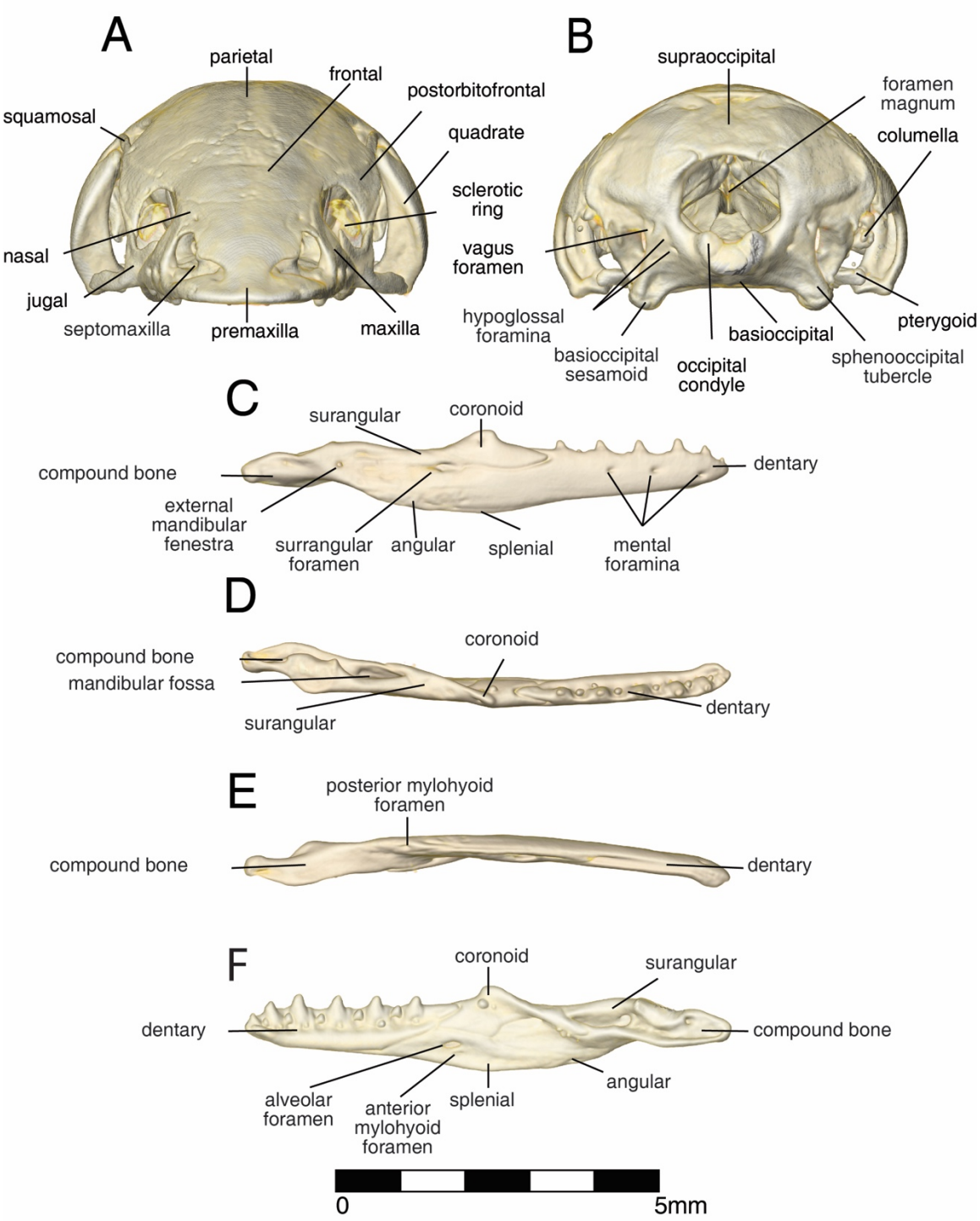

Figure 7. Individual bone segmentation of *Calyptommatus leiolepis* (MZUSP 71156) (1 of 8). Skull in (A) anterior and (B) posterior view, jaw in (C) lateral, (D) dorsal, (E) ventral, and (F) medial view.

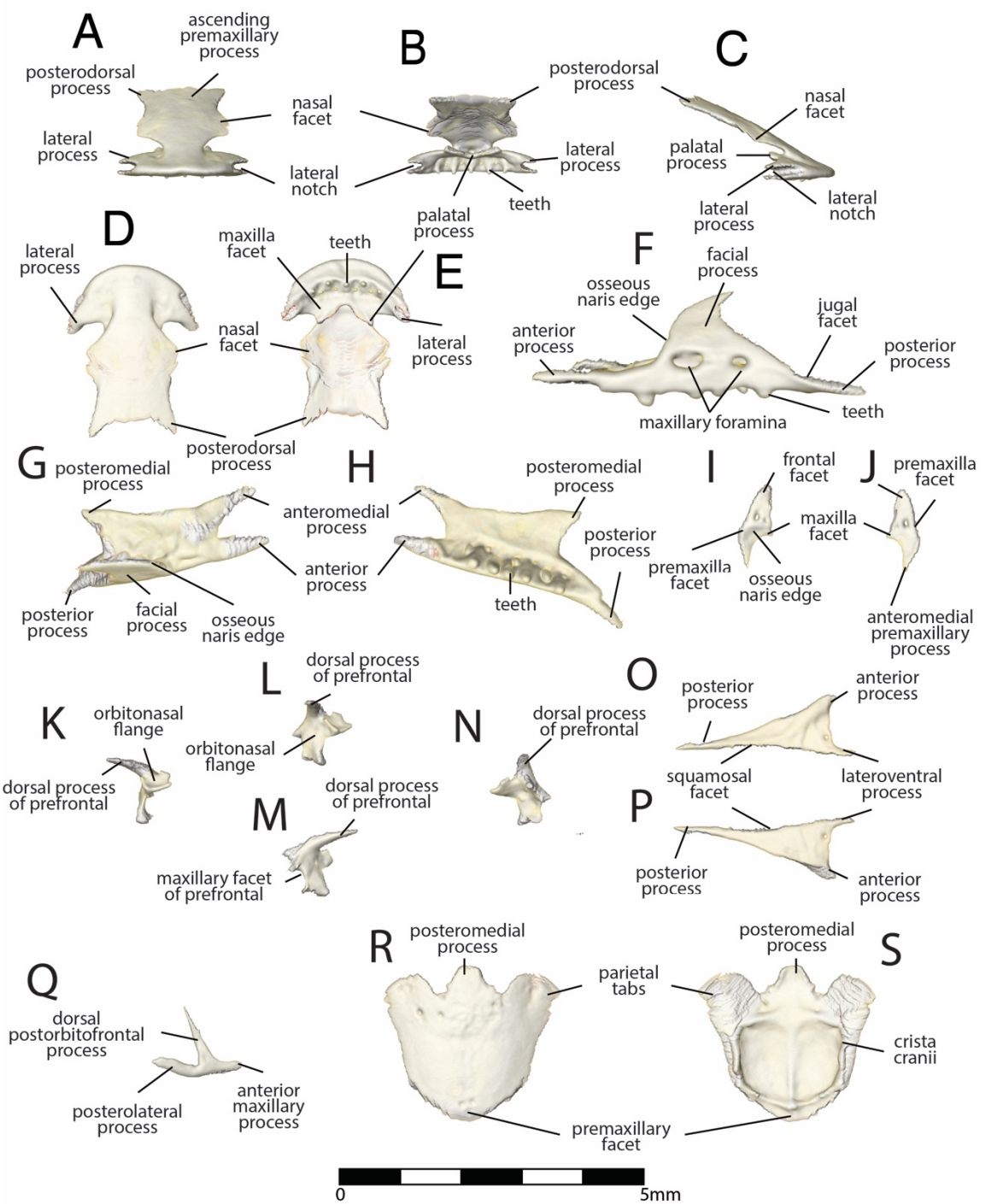

Figure 8. Individual bone segmentation of *Calyptommatus leiolepis* (MZUSP 71156) (2 of 8). Premaxilla in (A) anterior, (B) posterior, (C) lateral, (D) dorsal, and (E) ventral views. Left maxilla in (F) lateral view. Right maxilla in (G) dorsal and (H) ventral views. Right nasal in (I) dorsal and (J) ventral view. Left prefrontal in (M) medial, (N) posterior, (O) anterior, and (P) lateral views. Right postorbitofrontal in (K) medial and (L) lateral views. Right jugal in (Q) lateral view. Frontal in (R) dorsal and (S) ventral views.

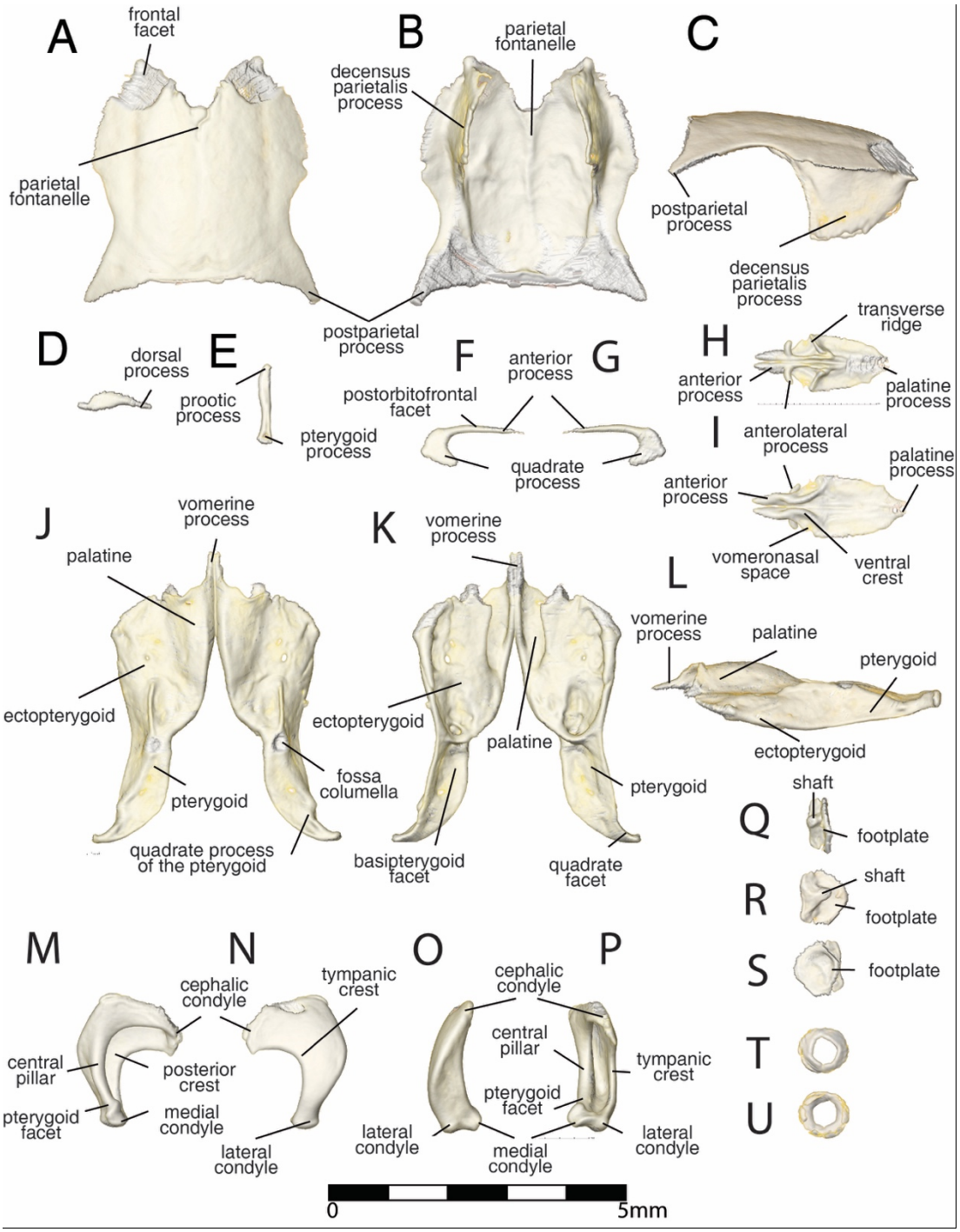

Figure 9. Individual bone segmentation of *Calyptommatus leiolepis* (MZUSP 71156) (3 of 8). Parietal in (A) dorsal, (B) ventral, and (C) lateral views. Right supratemporal in (D) dorsal view. Right epipterygoid in (E) medial view. Right squamosal in (F) lateral and (G) medial views. Vomer in (H) dorsal and (I) ventral view. Combined palatine, ectopterygoid, and pterygoid in (J) dorsal, (K) ventral, and (L) lateral views. Right quadrate in (M) medial, (N) lateral, (O) anterior, and (P) lateral views. Otostapes in (Q) anterior, (R) lateral, and (S) medial views. Right sclerotic ring in (T) lateral and (U) medial views.

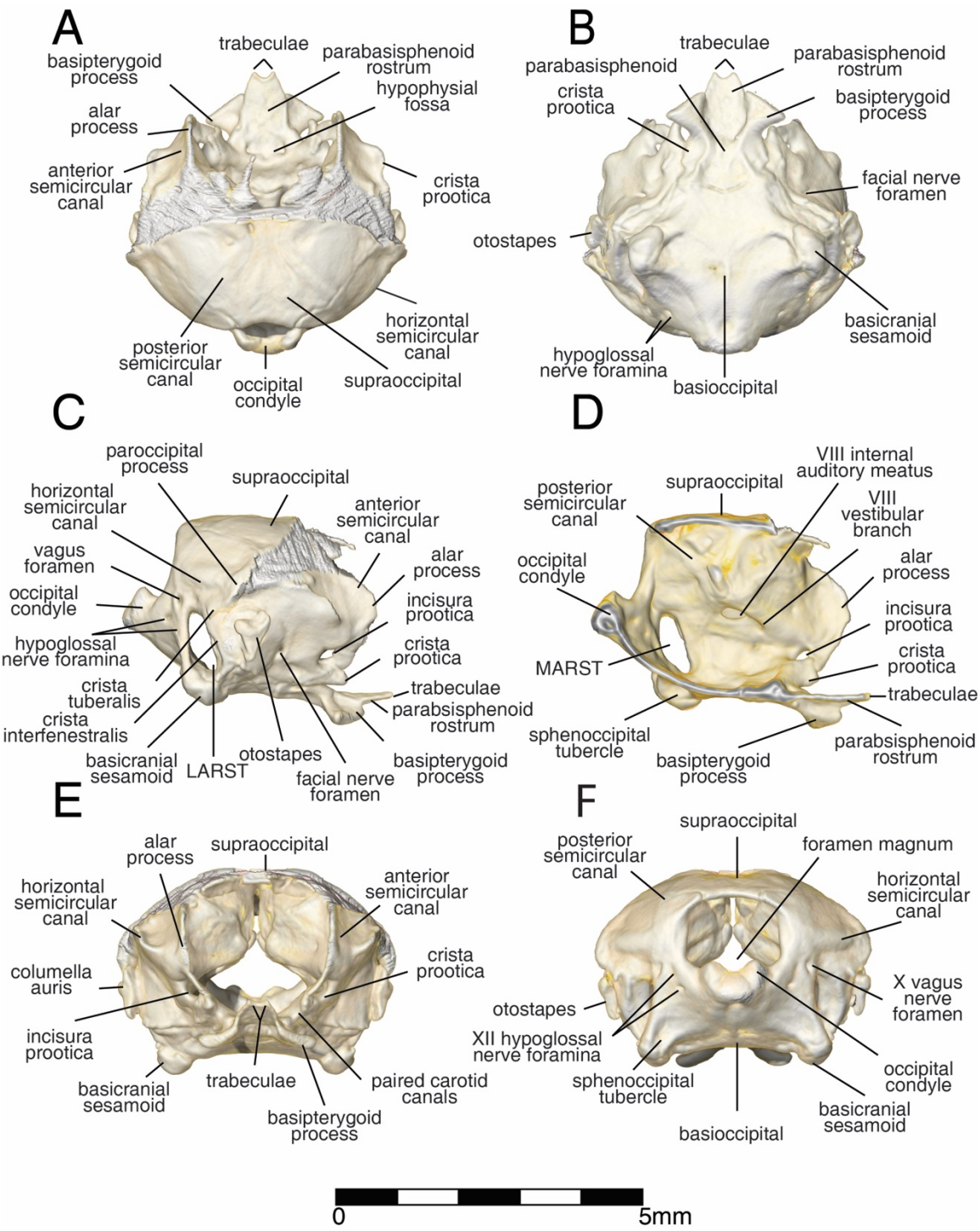

Figure 10. Individual bone segmentation of *Calyptommatus leiolepis* (MZUSP 71156) (4 of 8). Basicranium in (A) dorsal, (B) ventral, (C) lateral, (D) medial, (E) anterior, and (F) posterior views.

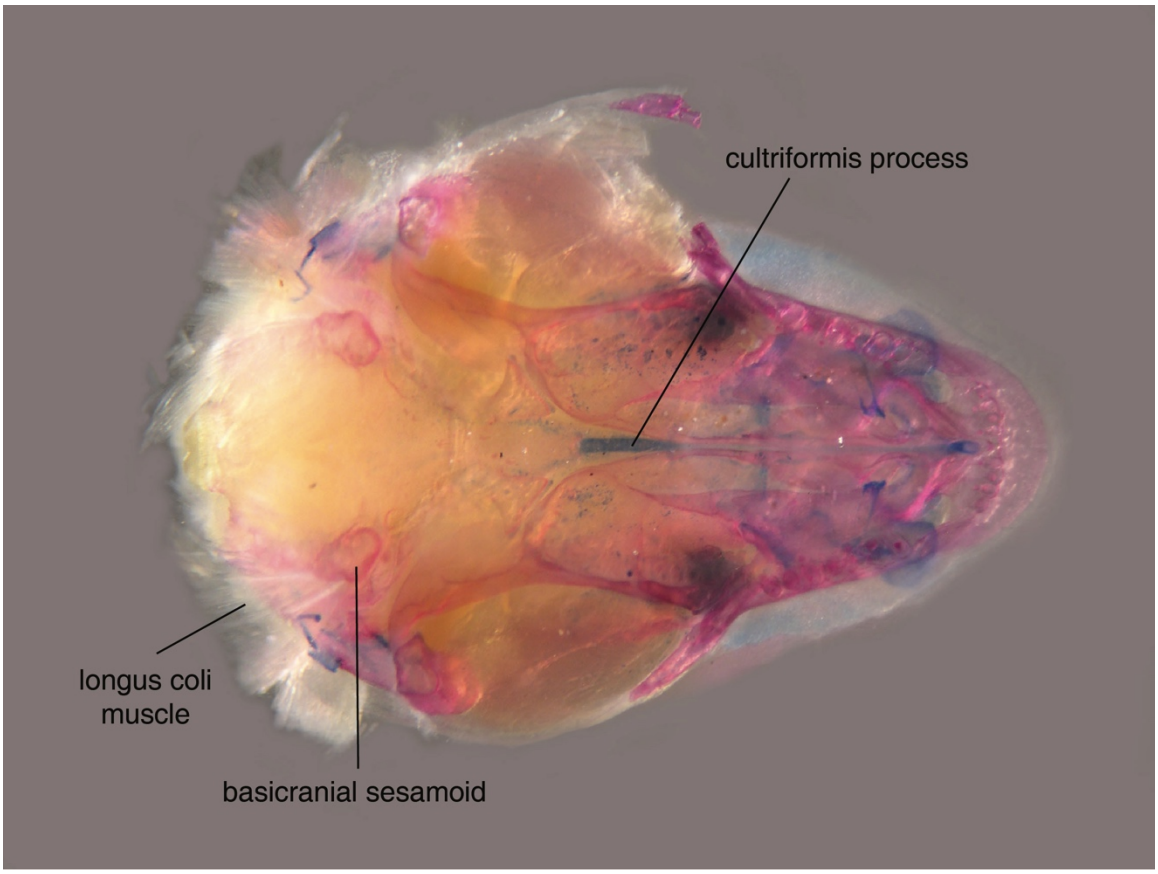

Figure 11. Cleared and stained *Calyptommatus leiolepis* (MZUSP 71156) in ventral view emphasizing the basicranial sesamoid and longus coli muscle.

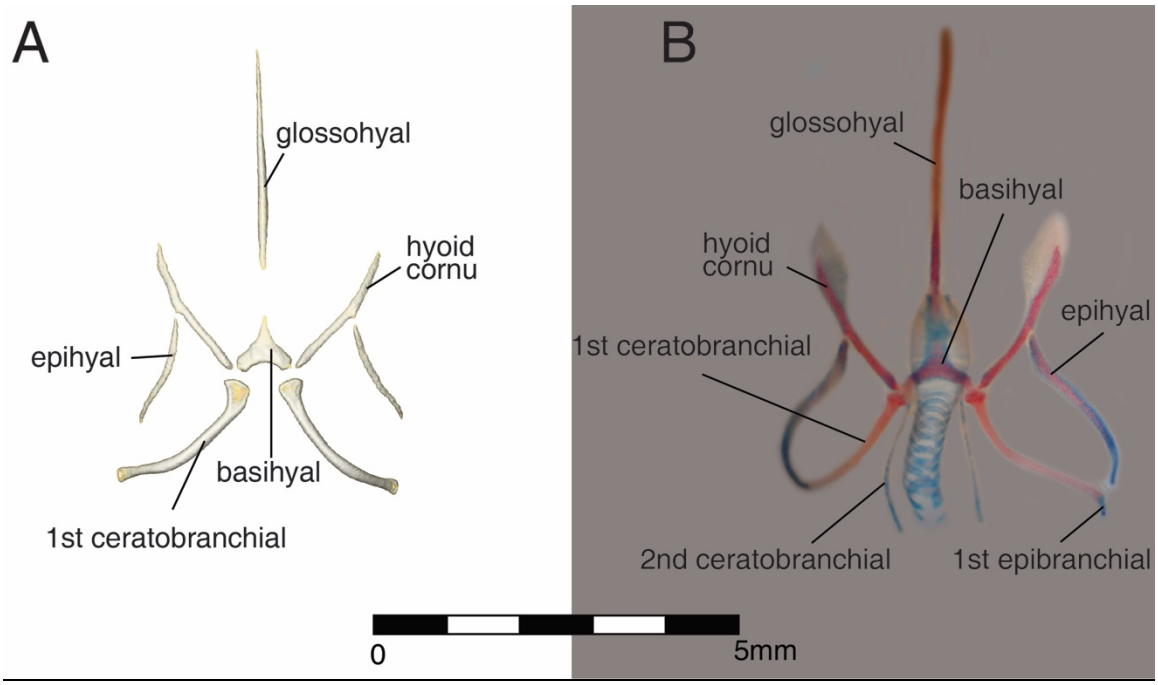

Figure 12. Ventral views of the individual bone segmentation (A) and histological staining (B) of the hyoid apparatus of *Calyptommatus leiolepis* (MZUSP 71156) (5 of 8).

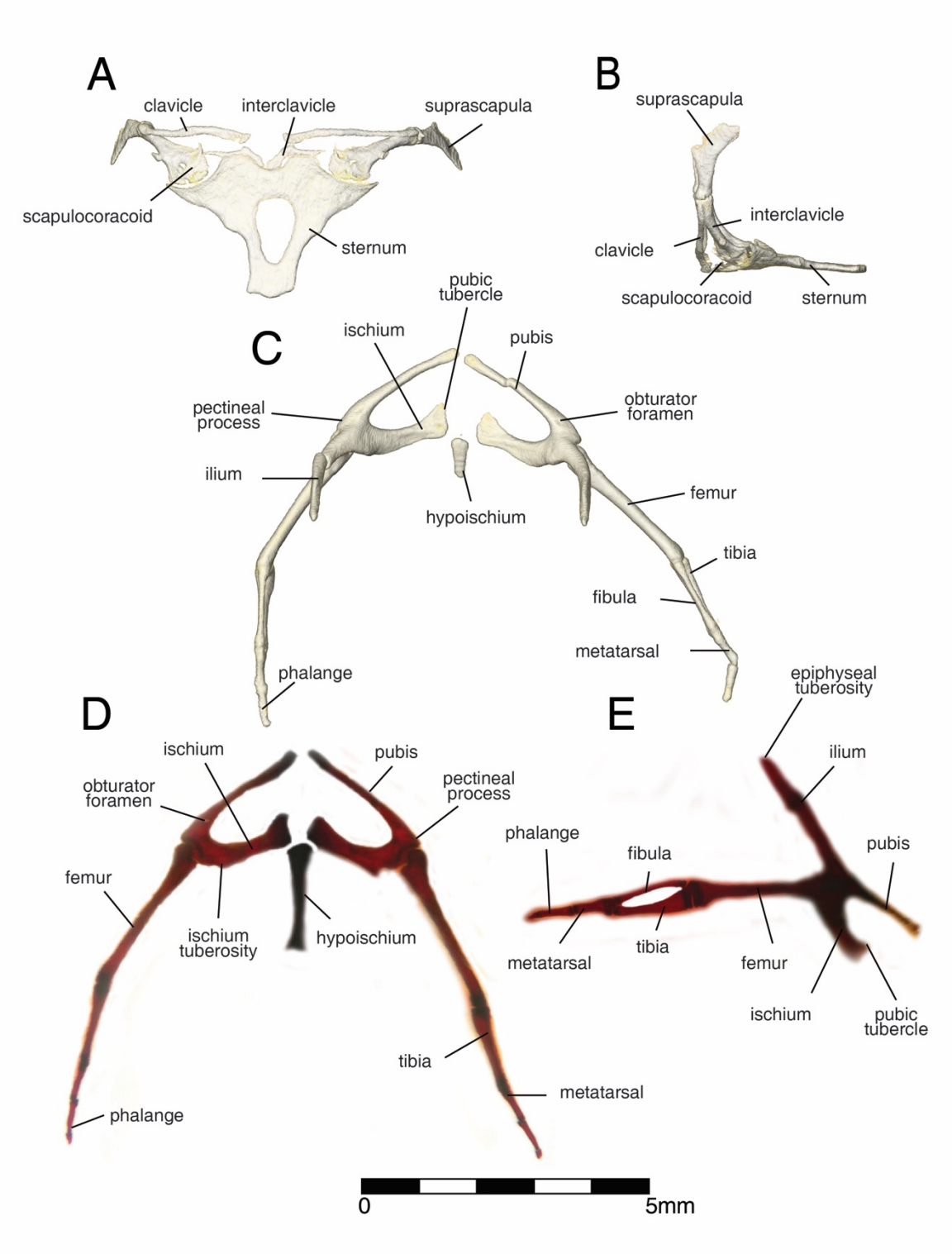

Figure 13. Individual bone segmentation and histological staining of *Calyptommatus leiolepis* (MZUSP 71156) (6 of 8). Pectoral girdle in (A) ventral and (B) lateral views. Bone segmentation of pelvic girdle in (C) dorsal view. Histological staining of pelvic girdle in (D) ventral and (E) lateral views.

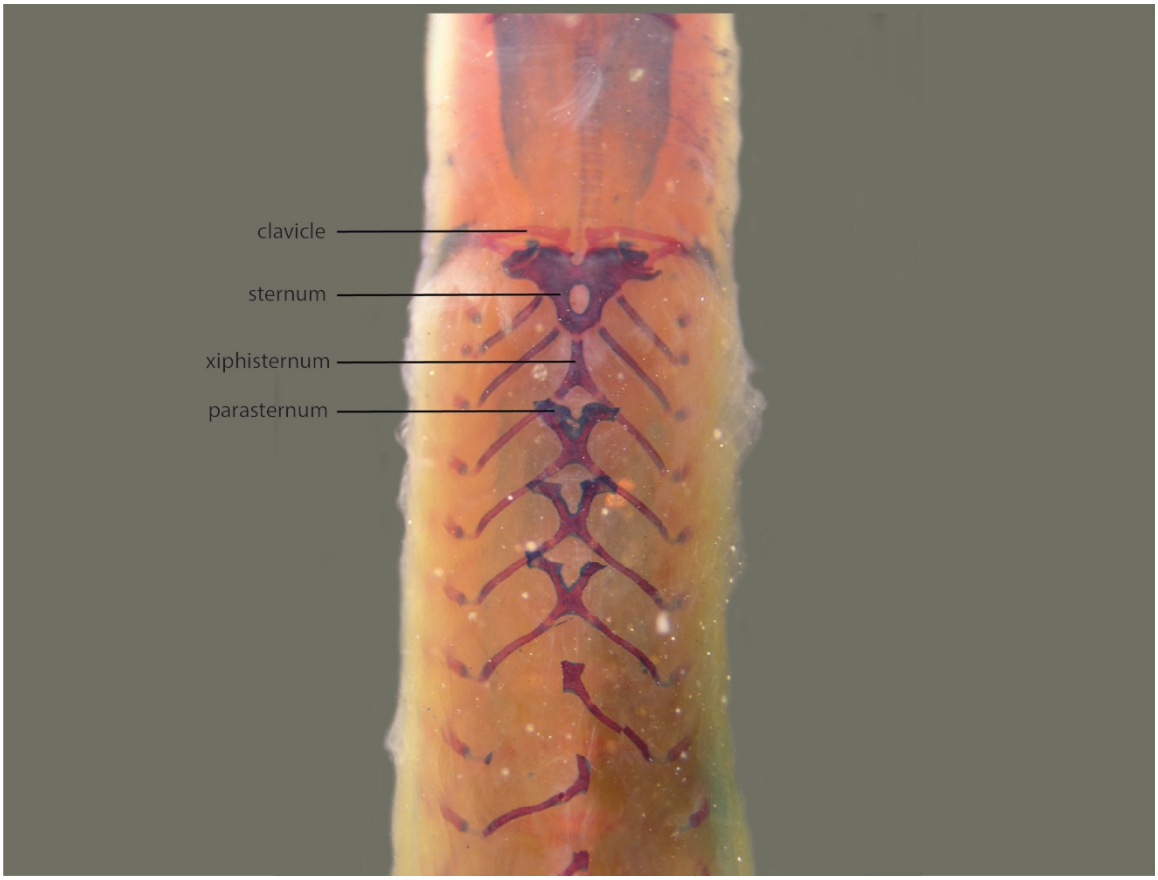

Figure 14. Cleared and stained specimen of *Calyptommatus leiolepis* (MZUSP 71156) emphasizing the parasternum in the pectoral girdle.

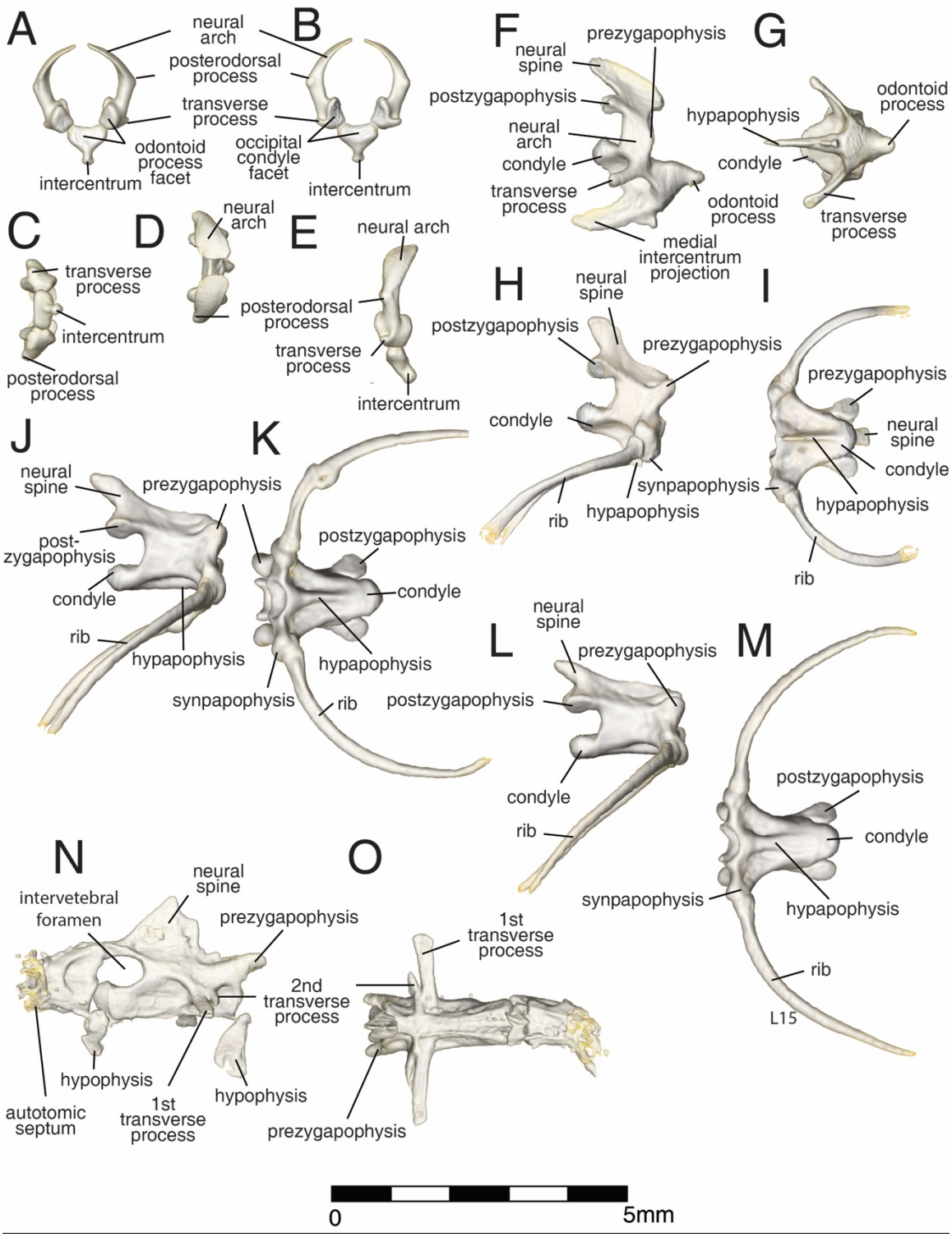

Figure 15. Individual bone segmentation of *Calyptommatus leiolepis* (MZUSP 71156) (7 of 8). Atlas in anterior (A), posterior (B), dorsal (C), lateral (D), and ventral (E) views. Axis in lateral (F) and ventral (G) views. Trunk vertebra 2 in lateral (H) and ventral (I) views. Trunk vertebra 12 in lateral (J) and ventral (K) views. Trunk vertebra 27 in lateral (L) and ventral (M) views. Caudal vertebra 3 in lateral (N) and ventral (O) views.

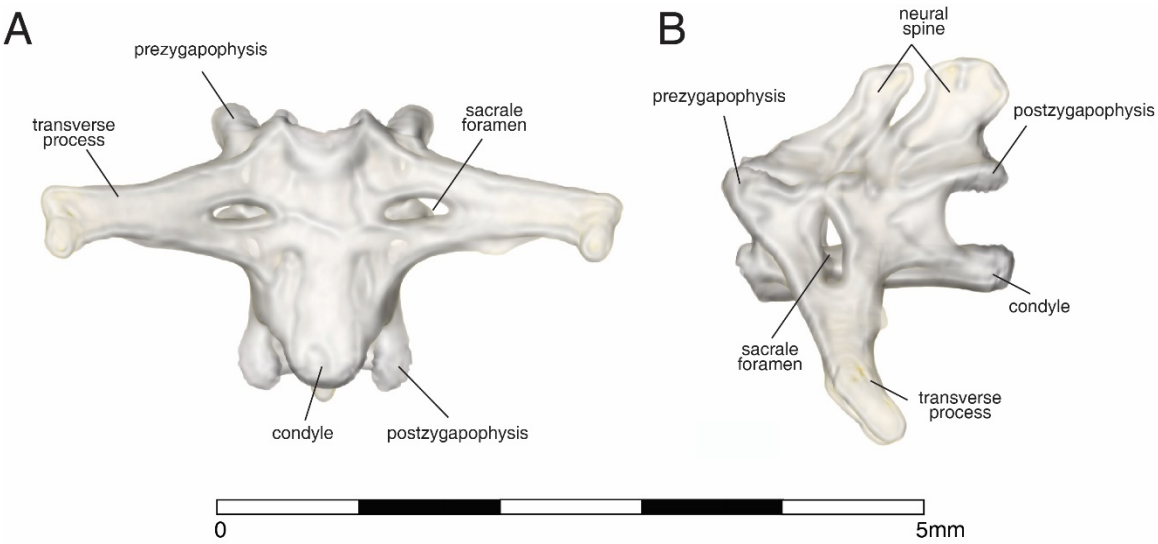

Figure 16. Individual bone segmentation of *Calyptommatus leiolepis* (MZUSP 71156) (8 of 8). Sacrum in ventral (A) and lateral (B) views.

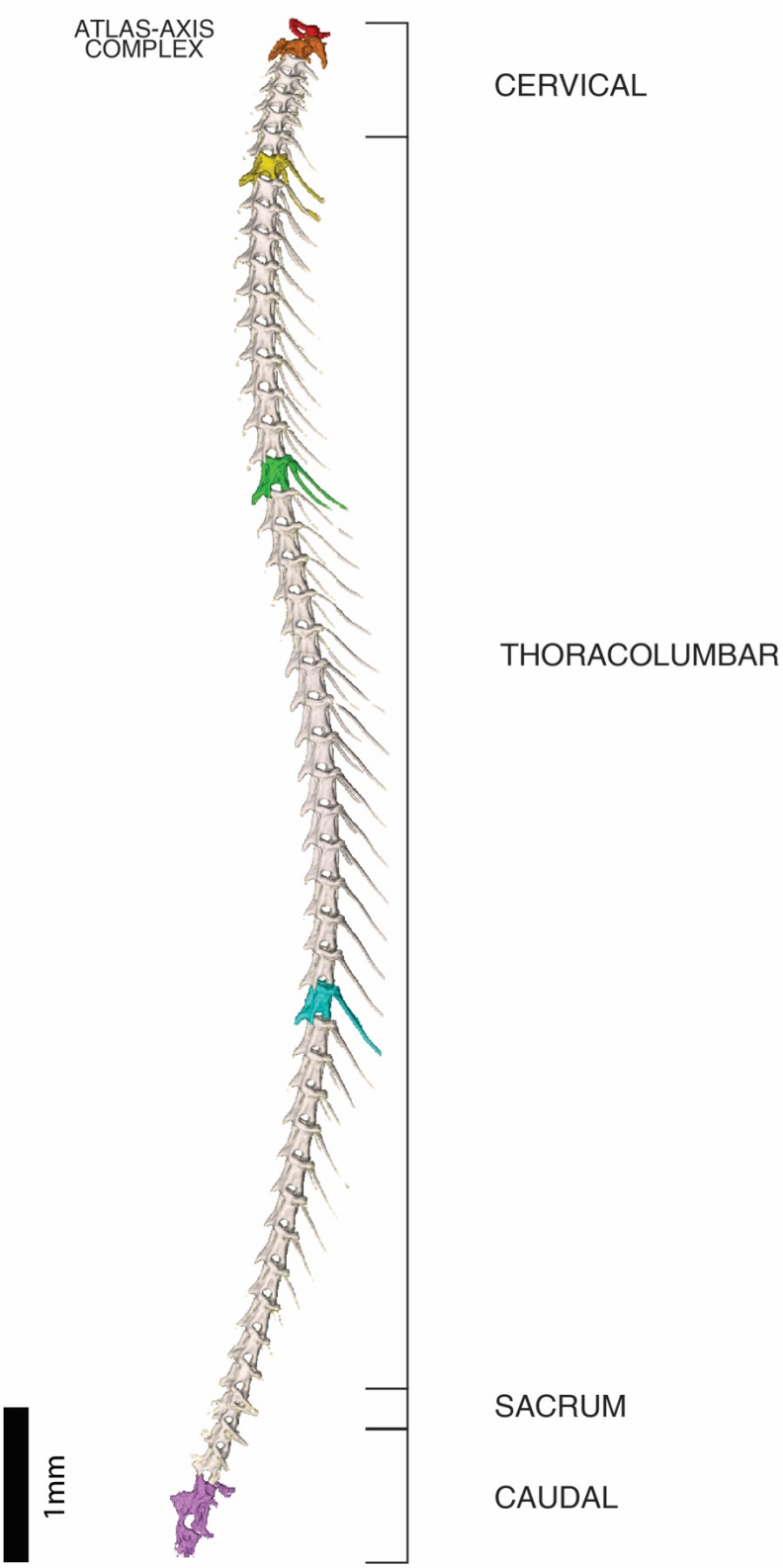

Figure 17. Complete vertebral segmentation and region identification of *Calyptommatus leiolepis* (MZUSP 71156).

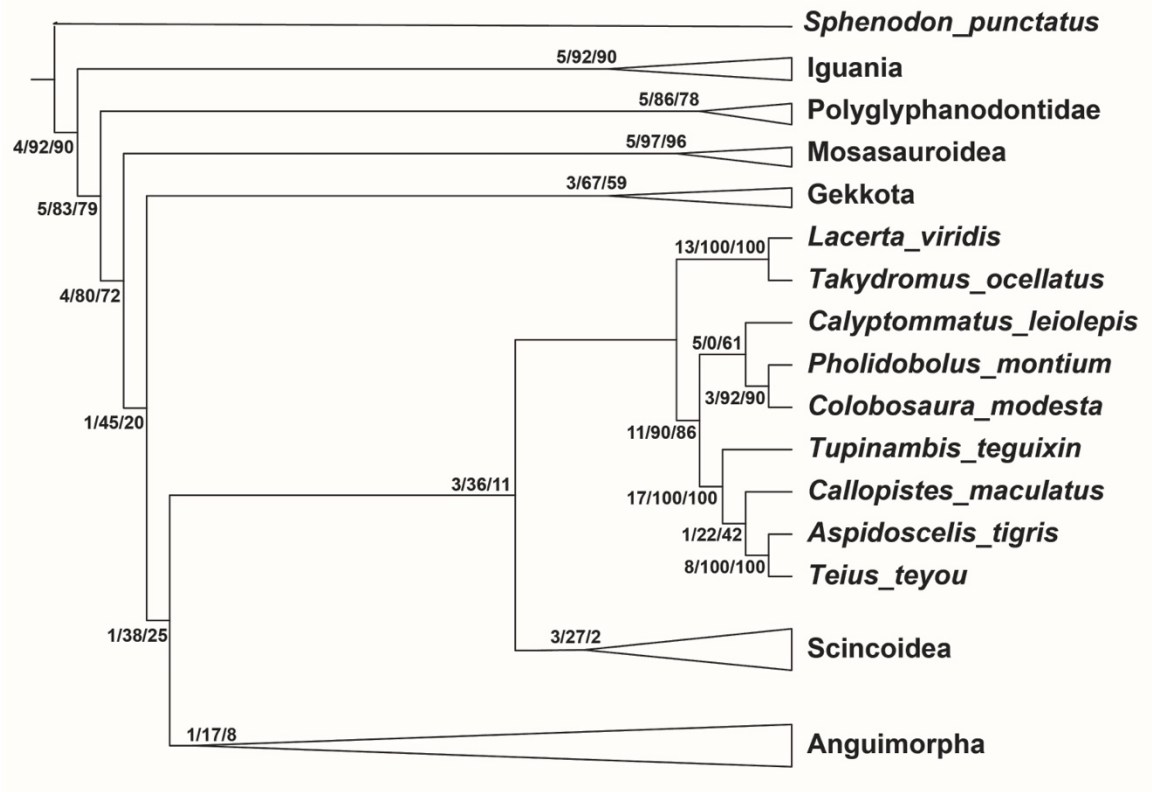

Figure 18. Maximum parsimony analysis of Squamata with the insertion of *Calyptommatus leiolepis* (MZUSP71156): support values indicated at each node Bremmer/relative Bremmer/bootstrap.

CHAPTER III

Discussion

Calyptommatus leiolepis comprises all characters representative of gymnophthalmids: fused frontals, loss of a parietal foramen and frontal lappets covering the parietal (Estes et al, 1988; Bell et al, 2003). Although these characters are common to gymnophthalmids, there is a large amount of variation within the group. Much of the variation within gymnophthalmids is found in the temporal and suborbital fenestrae, frontal, parietal, squamosal, palatal elements, presence or absence of lacrimals, postfrontals, postorbitals, tooth counts, and morphology of the jaw and braincase (Bell et al, 2003). *C. leiolepis* comprise many specialized characters that separate it from other taxa within gymnophthalmids as well as other limb-reduced groups. These characters include the head containing a shovel-like snout with a well-developed horizontal keel, nasal cartilages that produce a sand-guard to protect the nostrils, reduced eyes covered by a brille, lack of forelimbs, extreme reduction of hindlimbs, and imbricated scales among others.

Under closer examination using HRCT scan data, the snout of *C. leiolepis* is narrow, but when the whole specimen is visually examined it appears broad (Figure 2). This broadening of the snout is due to the specialized development of a cartilaginous rim that boarder the snout. This is a unique character that no other lizard contains and has allowed *C. leiolepis* to increase surface area without having to widen the bone.

The ocular skeleton of squamates has recently been found to be an important diagnostic character for fossorial squamates (Atkins and Franz-Odendaal, 2016). The ocular skeleton is comprised of a combination of scleral cartilage and ossicles (Walls,

1942). The presence or absence of these elements is variable among vertebrate groups and are thought to be influenced by behavior (Atkins and Franz-Odendaal, 2016). Groups that have a fossorial lifestyle and are scotopic, contain scleral ossicles that are reduced or absent (e.g., amphisbaenians), while those that are non-fossorial and photopic have well developed sclerotic rings (Franz-Odendaal, 2008). For *C. leiolepis*, individual scleral ossicles (~14) are present during early stages of development, but these elements become fused in the adult (Roscito and Rodrigues, 2012). Given the tendency of these lizards to burrow within sandy substrates, it is expected that they would correspond more with fossorial and scotopic animals. Loss of the ocular skeleton is a diagnostic character for fossorial taxa (Atkins and Franz-Odendaal, 2016), but this tendency has not been observed in *C. leiolepis* or any other sand-swimmer lizards like the African Sandfish (e.g., *Scincus scincus*), which has a similar ocular skeleton to C. *leiolepis* (i.e., fused elements). Additionally, there is a complete external brille covering the eye. This trait is found in many groups of squamates including members of the Pygopodidae, Gekkonidae, Phyllodactylidae, Scincidae, Sphaerodactylidae, Serpentes, and Gymnophthalmidae (Guerra-Fuentes et al., 2014).

The suborbital fenestra is almost lost within *C. leiolepis*. This finding is unusual due to the skeletal autapomorphy of having a suborbital fenestra is contained within all basal lineages of diapsids (Evans 1988). This character is usually made by the bone-to-bone contact between the palatine, ectopterygoid, and the maxilla. This characteristic of closing of the suborbital fenestra is even further exacerbated by a complete closure of the fenestra in *C. nicterus* (Roscito and Rodrigues, 2010).

Another finding includes that of the basicranial sesamoid, which is an ossified element that covers the sphenoccipital tubercle of the basicranium (Figure 9). In *C. leiolepis*, the element is large (~1mm) and globular shaped. Many other vertebrate groups contain sesamoids but these elements vary dramatically in shape and size depending on the taxa's degree of fossoriality (Montero et al., 2016). Within squamates, basicranial sesamoids have been found in many families, fossorial or not (Montero et al., 2016). Taxa that are not fossorial may or may not contain this element, but if this element is present it is usually reduced in size in n0n-fossorial taxa. *C. leiolepis* contains a proportionally large basicranial sesamoid (~1mm) compared to other non-fossorial taxa (Montero et al., 2016). This morphological adaptation towards a larger basicranial sesamoid may be attributed to assisting some of the head movement muscles during burrowing through the substrate. It has been shown that these basicranial sesamoids are anchors of attachment for the long coli muscle (Montero et al., 2016). The function of this muscle is for movement of the head in a ventral motion. Thus, a larger basicranial sesamoid would increase the surface area for attachment of the longus coli muscle for a greater force for burrowing.

The jugal is another diagnostic character for *Calyptommatus*, containing a triradiated morphology. Upon close examination, the posterolateral process is elongated with finger-like projections. This elongation of the posterolateral process of the jugal has been found in other squamate groups, being attributed to the redevelopment of the posttemporal bar (Mo et al., 2009).

Postorbitofrontal is a name that has been applied to the unique element on the posterodosal portion of the orbit in *Calyptommatus*, a similar situation occurs in some

iguanians, all gekkotans and anguids (Camp, 1923; Conrad, 2008; Daza and Bauer, 2010). In squamates, usually the bone that participates in the postorbital bar and the upper temporal bar is the postorbital, while the postfrontal usually clasps the frontoparietal suture (Evans, 2008). Developmental data for gekkotans have shown that in *Eublepharis macularius* the postorbitofrontal corresponds only to the postfrontal, but this interpretation is conditioned to an anterior shift of the postorbital to a parafrontal position and its successive fusion with the frontal bone (Wise and Russell, 2010). In *Calyptommatus* the postorbitofrontal is indeed formed by the fusion of a well-developed postorbital and reduced postfrontal (Roscito and Rodrigues, 2010).

Although *C. leiolepis* was described as lacking an external ear, it actually does contain a small opening visible in ventral view at the height of the bottom half of the fifth infralabial (Rodrigues, 1991). This opening is also seen in lateral view where a small tympanic membrane is visible, bounded by the posterior-most upper labials and below the second row of temporal scales. This ear opening is half the diameter of the eye. The presence of a tympanic membrane and the greater modification of the stapes suggest that this animal can perceive low frequency sounds and possible vibrations underground.

In extremely miniaturized lizards, the size of the foramina is commonly enlarged, seemingly the nerves and arteries that pierce them have to keep a minimum size after a certain point. For instance, the size of the maxillary foramina in Calyptommatus are huge compared with larger forms (e.g., *Neusticurus ecpleopus*; Bell et al., 2003).

Inherently, squamates encompass a very large diversity of body forms that range from fully tetrapod to the elongated limbless forms seen in snakes (Bradley et al., 2008; Vitt and Caldwell, 2008). This transition from having four fully-developed limbs to a

limbless form has been attributed to the modification of vertebral number as well as pectoral and pelvic girdle adaptations (Roscito and Rodrigues, 2013). Taxa that comprise a snake-like body form includes not just burrowing taxa, but surface and grass dwellers as well (Camp, 1923). The shift toward elongation of the trunk region is thought to have occurred due to the advantageous nature of undulatory locomotion, where movement through dense substrate would be hindered by fully developed limbs (Gans, 1974).

The pectoral and pelvic girdle is directly affected by the shift to a snake-like body form and comprises two patterns of reduction. The girdles can exhibit a greater reduction in the forelimb than the hind limb or have a greater reduction in the hind limb compared to the forelimb (Roscito and Rodrigues, 2013). For example, pygopodids contain taxa that are range from terrestrial and fossorial with varying degrees of girdle development (Greer, 1989). Terrestrial taxa contain well developed pectoral and pelvic girdles, in which the pelvic girdle becomes fused in the adult stage (Stephenson, 1962). Fossorial taxa on the other hand, have very reduced pelvic and pectoral girdle development, containing unfused pelvic elements (Stephenson, 1962; Greer, 1989). This theme also occurs within the families Scincidae and Gymnophthalmidae, where there are groups that contain well-developed girdle elements, but those that are fossorial are typically elongated with reduced girdle development (Greer, 1970). For *C. leiolepis*, the pelvic and pectoral girdles are very reduced, having unfused puboischiadic halves, reduction in size of pelvis (~4mm), and reduction of the prehensile elements in the hindlimb into one metatarsal and one phalange. These morphological adaptations are also characteristic in other burrowing taxa closely related to this taxon, such as *Scriptosaura catimbau* and *C. nicterus* (Roscito and Rodrigues, 2013).

Ancestral trunk vertebrae number is 25 (*Sphenodon punctatus*; Bergmann and Irschick, 2011). Lizard-like gymnophthalmids and some teiids have 25-26 trunk vertebrae, while snake-like species have an increased number of trunk vertebrae. Specifically, the vertebral column of *C. leiolepis* consists of 44 presacral vertebrae (Figure 15). Two modes of elongation have been determined: lengthening of the tail or of the trunk (Wiens and Slingluf, 2001; Wiens et al., 2006). The increased maneuverability of undulatory locomotion through the loose sand habitat in which *C. leiolepis* travels has led to the adaption of lengthening the trunk, but retaining a short/intermediate tail (unlike the “short-tailed burrowers”; Figure 1).

There is a longstanding problem in squamate phylogeny that creates major discrepancies in relationships among the major clades (i.e., Gekkota, Iguania, Scincomorpha, Anguimorpha, and Ophidia) based on morphology and molecular data (Losos et al., 2012). One main criticism to morphological data sets is that due to their shared missing appendicular elements, all the limb-reduced groups/body-elongated groups are clumped together in a “fossorial group” (Conrad 2008; Gauthier et al. 2012). *C. leiolepis* clearly demonstrates that not all fossorial and semi-fossorial taxa are affected and grouped together with limbless forms (other exceptions are pygopods geckos and the anguimorph *Ophisaurus*). *C. leiolepis* has an unique combination of derived characters that are diagnostic for this taxa (e.g., shovel-like snout with a well-developed horizontal keel, nasal cartilages, reduced eyes covered by a brille, lack of forelimbs, reduction of hind limbs, and imbricated scales), but at the same time this taxon still retains synapomorphies of gymnophthalmids. *C. leiolepis* has also developed adaptations for semi-fossorial dwelling, but these adaptations differ considerably with other fossorial

groups. To some extent, *C. leiolepis*, has reinvented its morphological blueprint to be compatible with its semi-fossorial lifestyle. This can be witnessed by comparing the way that the braincase becomes closed; in the majority of fossorial squamates groups, the parietal and the prootic form the main lateral walls of the braincase—in *C. leiolepis*, the decensus parietalis process of the parietal is hypertrophied, creating a robust structure for lateral protection, and fulfilling the protective function of the brain.

The genus *Calyptommatus* shows very unique morphological traits that are suitable for its sand swimming locomotion. The adaptations of these lizards represent well their habitat and behavior. This is a rare situation among squamates, where frequently their morphology is very generalized and establishing a relationship between ecology and morphology is very difficult. The in-depth study of the morphology of *C. leiolepis* suggests that these animals occupy an undescribed position in the lizard niche hypervolume (Pianka et al., 2017).

REFERENCES

Al-Hassawi, AM. 2007. Comparative anatomy of the neck region in lizards. Victoria, Canada: Trafford Publishing.

Arnold EN. 1998. Cranial kinesis in lizards: variations, uses, and origins. In: Hecht M, Macintyre R, Clegg M, editors. Evolutionary Biology Volume 30. New York: Plenum Press. pp323–357.

Atkins JB, Franz-Odendaal TA. 2016. The sclerotic ring of squamates: an evo-devo-eco perspective. Journal of Anatomy. 4:503–513.

Bell CJ, Evans SE, Maisano JA. 2003. The skull of the gymnophthalmid lizard *Neusticurus ecpleopus* (Reptilia: Squamata). Zoological Journal of the Linnean Society. 103:283–304.

Bever GS, Bell CJ, Maisano JA. 2005. The ossified braincase and cephalic osteoderms of *Shinisaurus crocodilurus* (Squamata, Shinisauridae). Palaentologia Electronica. 8:1–36.

Bradley MC, Huelsenbeck JP, Wiens JJ. 2008. Rates and patterns in the evolution of snake-like body form in squamate reptiles: evidence for repeated re-evolution of lost digits and long-term persistence of intermediate body forms. Evolution. 62:2042–2064.

Camp CL. 1923. Classification of the lizards. Bulletin of the American Museum of Natural History. 48:289–307.

Conrad JL. 2004. Skull, mandible, and hyoid of *Shinisaurus crocodilurus* Ahl (Squamata: Anguimorpha). Zoological Journal of the Linnean Society. 141:399–434.

Conrad JL. 2008. Phylogeny and systematics of Squamata (Reptilia) based on morphology. Bulletin of the American Museum of Natural History. 310:1–182.

Daza JD, Bauer AM. 2010. The circumorbital bones of the Gekkota (Reptilia: Squamata). The Anatomical Record: Advances in Integrative Anatomy and Evolutionary Biology. 293:402–413.

Etheridge R. 1967. Lizard caudal vertebrae. Copeia. 4:699–721.

Evans SE. 1988. The early history and relationships of the Diapsida. In: M.J. Benton , editor. The phylogeny and classification of the tetrapods. Oxford: Clarendon Press. pp 221–260.

Evans SE. 2008. The skull of lizards and tuatara. In: Gans C, Gaunt AS, Adler K, editors. Biology of the Reptilia, Volume 20, Morphology H. Ithaca. Society for the Study of Amphibians and Reptiles. pp 1–347.

Gans C. 1974. Biomechanics: An approach to vertebrate biology. Ann Arbor: University of Michagin Press.

Gans C. 1975. Tetrapod limblessness: evolution and functional corollaries. American Zoologist. 15:455–467.

Gauthier JA, Kearney M, Maisano JA, Rieppel O, Behlke ADB. 2012. Assembling the squamate tree of life: Perspectives from the phenotype and the fossil record. Bulletin of the Peabody Museum of Natural History. 53:3–308.

Greer AE. 1970. A subfamilial classification of scincid lizards. Bulletin of the Museum of Comparative Zoology. 139:151–184.

Greer AE. 1989. The biology and evolution of Australian lizards. Chipping Norton, Australia: Surrey Beatty and Sons.

Goloboff PA, Catalano SA. 2016. TNTversion 1.5, including a full implementation of phylogenetic morphometrics. Cladistics. 32:221–238.

Greene HW, Cundall D. 2000. Limbless tetrapods and snakes with legs. Science. 287:1939–1941.

Guerra C, Montero R. 2009. The skull of *Vanzosaura rubricauda* (Squamata: Gymnophthalmidae). Acta Zoologica (Stockholm). 90:359–371.

Guerra-Fuentes RA, Roscito JG, Nunes PM, Oliveira-Bastos PR, Antoniazzi MM, Jared C, Rodrigues MT. 2014. Through the Looking Glass: The Spectacle in Gymnophthalmid Lizards. The Anatomical Record. 297:496–504.

Hoffstetter R, Gasc JP. 1969. Vertebrae and Ribs of Modern Reptiles. In: Gans C, Bellairs A, Parsons TS, editors. Biology of the reptilia, Volume 1, Morphology A. New York. Academic Press London and New York. pp 1–373.

Jerez A, Mangione S, Abdala V. 2010. Occurrence and distribution of sesamoid bones in squamates: a comparative approach. Acta Zoologica (Stockholm). 91:295–305.

Kearney M, Stuart BL. 2004. Repeated evolution of limblessness and digging heads in worm lizards revealed by DNA from old bones. Proceedings of the Royal Society of London, Series B. 271:1677–1683.

Lakjer T. 1927. Studien über die Gaumenregion bei Sauriern im Vergleich mit Anamniern und primitiven Sauropsiden. Zoologische Jahrbucher Abteilung fuer Anatomie und Ontogenie der Tiere. 49:57–356.

Lambertz M. 2010. Kommentierte Liste der squamaten Reptilien des Sanddünengebietes am mittleren Rio São Francisco (Bahia, Brasilien) unter besonderer Berücksichtigung endemischer Faunenelemente. Ophidia. 4:2–17.

Lee MSY. 1998. Convergent evolution and character correlation in burrowing reptiles: towards a resolution of squamate relationships. Biological Journal of the Linnean Society. 65:369–453.

Losos, JB, Hillis DM, Greene HW. 2012. Who Speaks with a forked tongue? Science. 338:1428–1429.

Maisano, JA. 2008. A protocol for clear and double-staining squamate specimens. Herpetological Review. 39:52–54.

Mo JY, Xu X, Evans SE. 2009. The evolution of the lepidosaurian lower temporal bar: new perspectives from the Late Cretaceous of South China. Proceedings of the Royal Society. 277:331–336.

Ronquist F, Huelsenbeck JP. 2003. MrBayes 3: Bayesian phylogenetic inference under mixed models. Bioinformatics. 19:1572–1574.

Oelrich TM. 1956. The anatomy of the head of *Ctenosaurapectinata* (Iguanidae). University of Michigan Museum of Zoology, Miscellaneous Publications. 94:1–122.

Pellegrino KCM, Rodrigues MT, Yonenaga-Yassuda Y, Sites JW. 2001. A molecular perspective on the evolution of microteiid lizards (Squamata, Gymnophthalmidae), and a new classification for the family. Biological Journal of the Linnean Society. 74:315–338.

Pianka ER, Vitt LJ, Pelegrin N, Fitzgerald DB, Winemiller KO. 2017. Toward a Periodic Table of Niches, or Exploring the Lizard Niche Hypervolume. The American Naturalist. 190:601–616.

Pyron RA, Burbrink FT, Wiens JJ. 2013. A phylogeny and revised classification of Squamata, including 4161 species of lizards and snakes. BMC Evolutionary Biology. 13:93.

Rieppel O. 1984a. Miniaturization of the lizard skull: Its functional and evolutionary implications. In: Ferguson MWJ, editor. The Structure, Development and Evolution of Reptiles. London: The Zoological Society of London, Academic Press. pp 503–520.

Rieppel O. 1984b. The structure of the skull and jaw adductor musculature of the Gekkota, with comments on the phylogenetic relationships of the Xantusiidae (Reptilia: Lacertilia). Zoological Journal of the Linnean Society. 82:291–318.

Rieppel O. 1985. The recessus scalae tympani and its bearing on the classification of reptiles. Journal of Herpetology. 19:373–384.

Rieppel O. 1994. The Lepidosauromorpha: an overview with special emphasis on the Squamata. In: Fraser NC, Sues H-D, editors. In the Shadow of the Dinosaurs: Early Mesozoic Tetrapods. New York: Cambridge University Press. pp 23–37.

Rieppel O. 1996. Miniaturization in tetrapods: Consequence for skull morphology. In: Miller PJ, editor. Miniature Vertebrates: The Implications of Small Body Size. Symposia of the Zoological Society of London 69. New York: Oxford University Press. pp 47–61.

Rieppel O, Gauthier J, Maisano JA. 2008. Comparative morphology of the dermal palate in squamate reptiles, with comments of phylogenetic implications. Zoological Journal of the Linnean Society. 152:131–152.

Robinson PL. 1967. The evolution of the Lacertilia. In: Problèmes actuels de paléontologie: Évolution des vertébrés. Paris: Actes du colloque international Centre national de la recherche scientifique. 163:395–407.

Rodrigues MT. 1991. Herpetofauna das dunas interiores do Rio São Francisco, Bahia, Brasil. I. Introdução à área e descrição de um novo gênero de microteiideos (*Calyptommatus*) com notas sobre sua ecologia, distribuição e especiação (Sauria, Teiidae). Papéis Avulsos de Zoologia. 37:285–320.

Roscito JG, Rodrigues MT. 2010. Comparative cranial osteology of fossorial lizards from the tribe Gymnophthalmini (Squamata, Gymnophthalmidae). Journal of Morphology. 271:1352–1365.

Roscito JG, Rodrigues MT. 2013. A Comparative Analysis of the Post-Cranial Skeleton of Fossorial and Non-Fossorial Gymnophthalmid Lizards. Journal of Morphology. 274:845–858.

Sanger TJ, Gibson-Brown JJ. 2004. The Developmental Bases of Limb Reduction and Body Elongation in Squamates Evolution. 58: 2103–2106.

Siedchlag AC, Benozzati ML, Passoni JC, Rodrigues MT. 2010. Genetic structure, phylogeny, and biogeography of brazilian eyelid-less lizards of genera *Calyptommatus* and *Nothobachia* (Squamata, Gymnophthalmidae) as inferred from mitochondrial DNA sequences. Molecular Phylogenetics and Evolution. 56:622–630

Tarazona OA, Fabrezi M, Ramírez-Pinilla MP. 2008. Cranial morphology of *Bachia bicolor* (Squamata: Gymnophtalmidae) and its postnatal development. Zoological Journal of the Linnean Society. 152:775–792.

Uetz P, Hošek J, Hallermann J. 2018. The Reptile Database. Available at http://www.reptiledatabase.org. In.

Vitt LJ, Caldwell JP. 2008. Herpetology, third edition: An introductory biology of amphibians and reptiles, 3 ed: Academic Press.

Wiens JJ. 2004. Development and evolution of body form and limb reduction in squamates: A response to Sanger and Gibson-Brown. Evolution. 58:2107–2108.

Wiens JJ, Brandley MC, Reeder TW. 2006. Why does a trait evolve multiple times within a clade? Repeated evolution of snakelike body form in squamate reptiles. Evolution. 60:123–141.

Wiens JJ, Slingluff JL. 2001. How lizards turn into snakes: A phylogenetic analysis of body form evolution in anguid lizards. Evolution. 55:2303–2318.

Wise PAD, Russell AP. 2010. Development of the dorsal circumorbital bones in the leopard gecko (Eublepharis macularius) and its bearing on the homology of these elements in the Gekkota. Anatomical Record. 293:2001–2006.

Zaher H, Apesteguía S, Scanferla CA. 2009. The anatomy of the Upper Cretaceous snake Najash rionegrina Apesteguía & Zaher, 2006, and the evolution of limblessness in snakes J. Zoological Journal of the Linnean Society. 156:801–826.

VITA

Nicholas Theodore Holovacs

Sam Houston State University, Department of Biological Sciences, 1900 Avenue I, Huntsville, TX 77341 USA

Education

M. Sc. Sam Houston State University, Department of Biological Sciences.
Fall 2016 – Summer 2018. Major: Biology

B.Sc. Sam Houston State University, Department of Biological Sciences (Huntsville, Texas). Major: Biology/ Minor: Chemistry.

Main research project:
Morphological adaptations of the sand-swimmer lizard *Calyptommatus leiolepis* (Squamata: Gymnophtalmidae).

Teaching Experience

Sam Houston State University, Department of Biological Sciences, Huntsville USA. Head Laboratory Instructor of the Human Anatomy and Physiology Course (BIO–2403) for medical oriented career paths. Fall 2017-Spring 2018. Enrolled Students: ~50. Duties and responsibilities: Lecture, grading, and assisting students during office hours.

Sam Houston State University, Department of Biological Sciences, Huntsville USA. Head Laboratory Instructor of the Human Physiology Course (BIO–2402) for medical oriented career paths. Summer 2016 – Summer 2017. Enrolled Students: 50 – 200 (depending on academic semester). Duties and responsibilities: Lecture, grading, and assisting students during office hours.

Sam Houston State University, Department of Biological Sciences, Huntsville USA. Lab Instructor of the Cellular Biology Course (BIO–2440). Spring 2017. Enrolled Students: 25. Duties and responsibilities: Lecture, grading, and assisting students during office hours.

Sam Houston State University, Department of Biological Sciences, Huntsville USA. Volunteer Laboratory Instructor of the Herpetology Course (BIO–5383 and BIO–4096) for Graduate and Undergraduate students. Spring 2016. Enrolled Students: 12. Helped the students creating 3D animations of CT scan data. Helped setting up the practical test and attended lectures, field trips and helped preserving specimens.

Sam Houston State University, Department of Biological Sciences, Huntsville USA. Laboratory Instructor of the Comparative Vertebrate Anatomy Course (BIO–3450) for medical oriented career paths. Fall 2015. Enrolled Students: 10. Duties and responsibilities: Lecture, grading, and assisting students during office hours.

Fellowships, Scholarships and Grants

Fall 2016 Sam Houston State University, Graduate Teaching Assistantship
Fall 2015 Sam Houston State University, Dr. Sam Barnes Kaplan Review Scholarship

Active Research Interests

Anatomy and systematics of living and extinct reptiles (focus on lizards, snakes and turtles).

Morphology, CT scans, Functional Morphology, Phenotypic and Genotypic Evolution, phylogenetic theory, evolutionary theory, evolutionary bioinformatics and computational phylogenetics.

Research Experience

Sam Houston State University, Huntsville, TX. Sampled microbial colonies on cadavers as microbiome changes throughout each season, to find a more accurate time of death for forensic science. Sampling was done at STAFS Body Farm. Biology Project. Fall 2014 – Spring 2015. Project heads: Dr. Aaron Lynne and Dr. Sibyl Bucheli.

Sam Houston State University, Huntville, TX. Used Contrast-Enhanced Micro-CT to visualize the cranial and jaw musculature of *Lemur catta* and describe the exact origin/insertion, as well as cooperative muscle fiber groups, within these muscle groups to more accurately discern bite force. Biology Project. Spring 2015. Project heads: Dr. Monte L. Thies and Dr. Juan D. Daza.

Sam Houston State University, Huntsville, TX. Used Contrast-Enhanced Micro-CT to study the morphological adaptations of the sand swimmer lizard *Calyptommatus leiolepis* (Squamata: Gymnophtalmidae). (In Preparation for the Anatomical Record).

Awards and Distinctions

Fall 2016 – Spring 2018: SHSU Teaching Assistantship (*Department of Biological Sciences*)
SHSU Institutional Honors: Cum Laude
Fall 2015: SHSU Dean's List
Spring 2015: SHSU President's List
Fall 2014: SHSU Dean's List
Fall 2013: SHSU Dean's List

Professional and Society Memberships

June 2017 – Present, Royal Microscopy Society member
August 2017 – August 2018, SHSU Biological Sciences Graduate Student Organization Treasurer
Fall 2016 – August 2018, SHSU Biological Sciences Graduate Student Organization
Spring 2016, Golden Key International Honour Society.
Spring 2014 – 2015, Sam Houston Association of Medically Oriented Students (2014: Treasurer, 2015: President)

Publications

Bauer AM, Beach-Mehrotra M, Bermudez Y, Clark GE, Daza JD, Glynne E, Hagyari D, Harnden JM, **Holovacs N**, Kanasiro A, Lofthus A, Pierce ZW, Aaliyah R, Syed S, Vallejo-Pareja MC, Walker BA and Willett J. The Tiny Skull of the Peruvian Gecko Pseudogonatodes barbouri (Gekkota: Sphaerodactylidae) Obtained via a Divide-And-Conquer Approach to Morphological Data Acquisition. South American Journal of Herpetology, 13(1):102–116.

Publications in Preparation

Daza JD, **Holovacs N**, Stanley E., Montero R, Guerra C. Morphological adaptations of the sand-swimmer lizard *Calyptommatus leiolepis* (Squamata: Gymnophtalmidae). (In Preparation for the Anatomical Record).

Participation in Conferences

Holovacs N, Daza JD, and Monte T. Description of the Cranial Jaw Musculature of *Lemur catta* Using Contrast-Enhanced Micro-CT. Department of Biological Sciences, Sam Houston State University, Huntsville, TX. Eighth Undergraduate Research Symposium. April 15, 2015. Poster Presentation.

Daza JD, **Holovacs N**, Thies ML, Lewis PJ, Green D. Disecando lagartos con el mouse: tomografías computarizadas usando contraste de yodo diffusible. XVI Congreso Argentino De Herpetología. San Miguel de Tucumán, Argentina. September 29 – October 2, 2015.

Daza JD, **Holovacs N**, Stanley EL, Guerra C, Montero R. El esqueleto de *Calyptomatus leiolepis* (Squamata, Gymnophthalmidae): Una mirada digital. XVI Congreso Argentino De Herpetología. San Miguel de Tucumán, Argentina. September 29 – October 2, 2015.

119th Annual Meeting of the Texas Academy of Science. March 4 – 6, 2016. Attended.

Daza JD, **Holovacs N**, Stanely EL, Guerra C, Montero R. El esqueleto de *Calyptomatus leiolepis* (Squamata, Gymnophthalmidae): Una mirada Digital. The American Society of Ichthyologists and Herpetologists (ASIH). New Orleans, Louisiana, 6 - 10 July 2016.

Annual Meeting of the Royal Microscopy Society ToScA Conference. June 5 – 8, 2017. Attended.

Technical Training

Proficient in Avizo 3D Software | FEI Software, Quicktime Pro, ImageJ RSB, Geneious, Mesquite v. 3.40, TNT v. 1.5, Minitab and SPSS statistical packages.

Written and Spoken Languages

English (Fully-English Proficient).

References

Dr. Juan D. Daza
Assistant Professor
Department of Biological Sciences
Sam Houston State University
Huntsville, Texas 77341
(936) 294-4250
daza@shsu.edu

Dr. Monte L. Thies
Professor
Department of Biological Sciences
Sam Houston State University
Huntsville, Texas 77341
(936) 294-3746
woodrat@shsu.edu

Dr. Sibyl R. Bucheli
Assistant Professor
Department of Biological Sciences
Sam Houston State University
Huntsville, Texas 77341
(936) 294-1554
bucheli@shsu.edu